SPETTROSCOPIA GAMMA

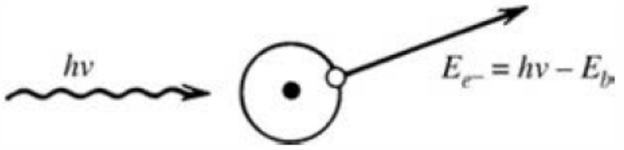

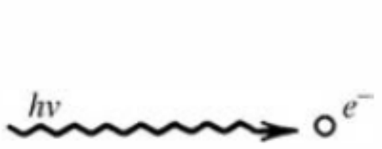

Before

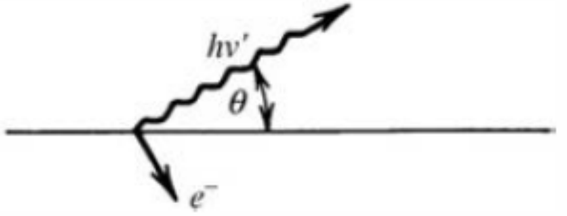

After

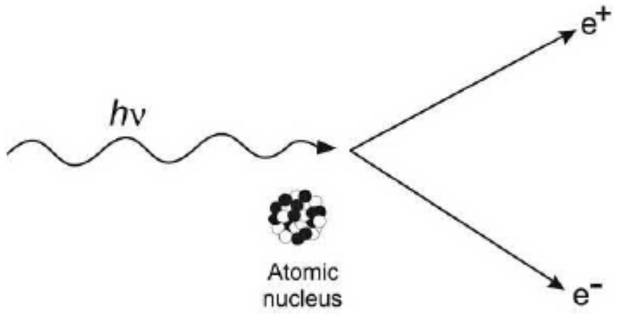

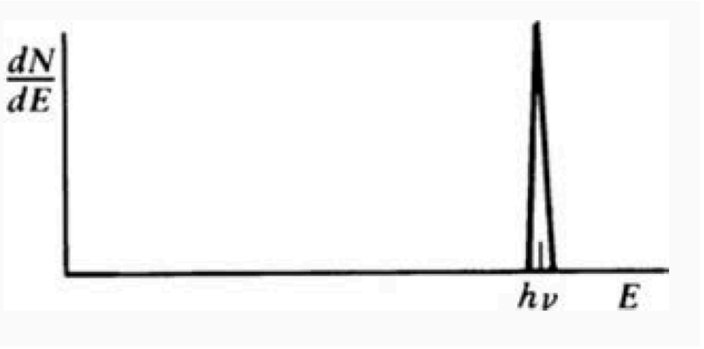

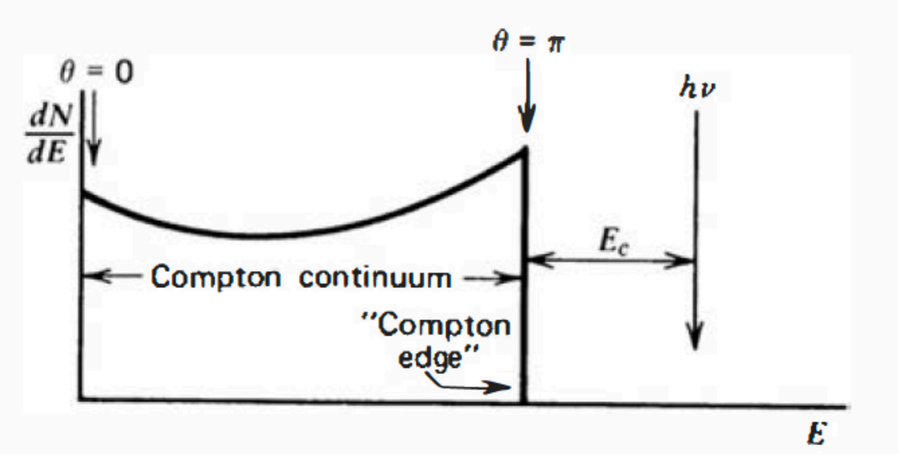

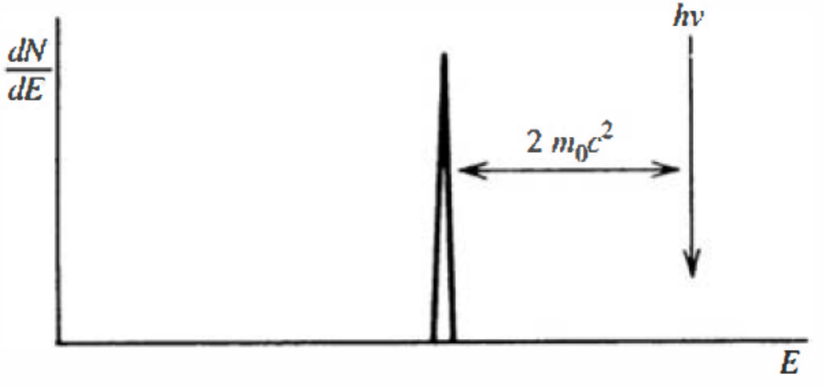

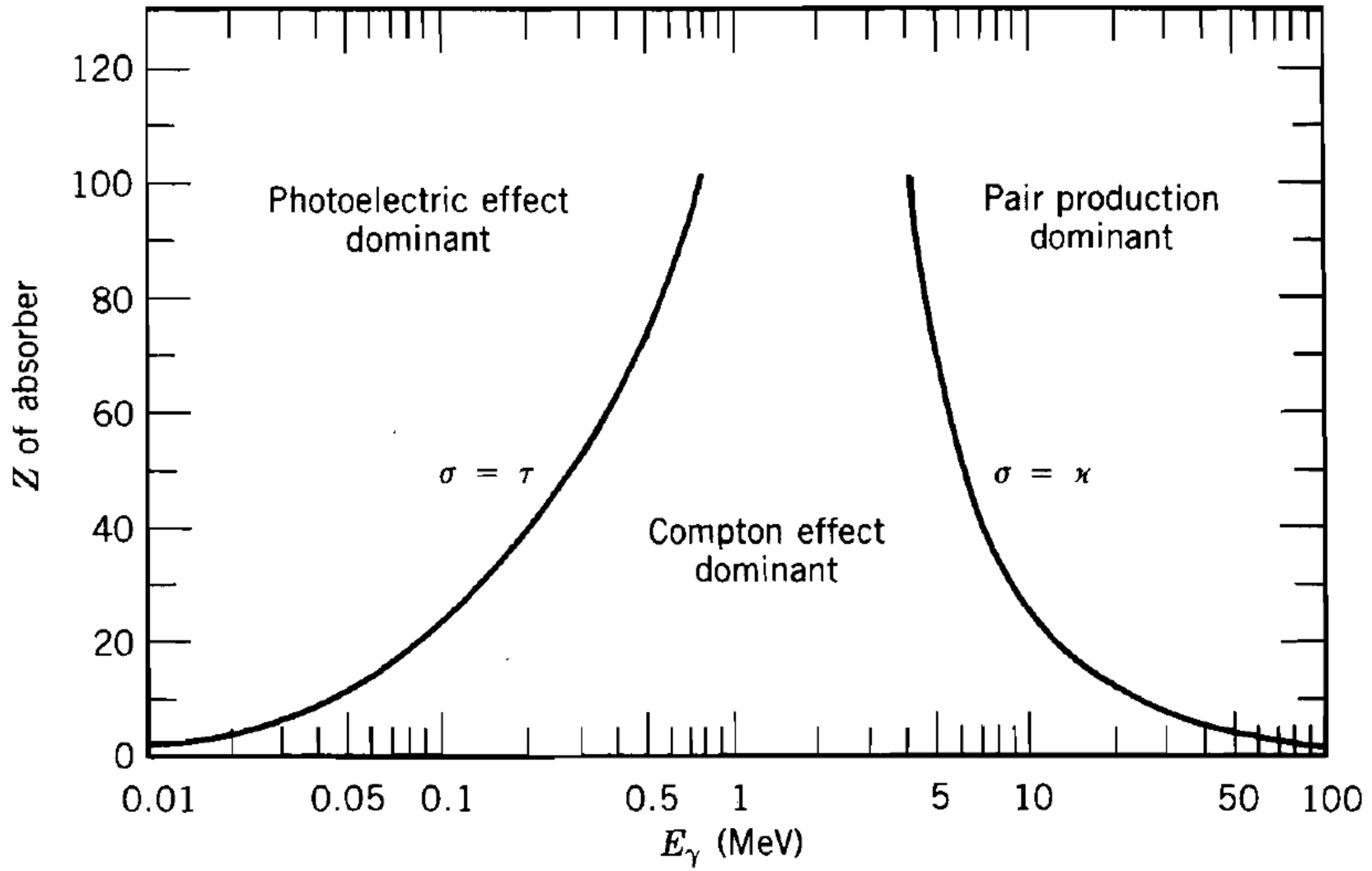
120
100
80
60
40
20
0
Z of absorber
Photoelectric effect
dominant
Pair production
dominant
$\sigma = \tau$
$\sigma = \kappa$
Compton effect
dominant
0.01
0.05
0.1
0.5
1
5
10
50
100
E_γ (MeV)

Rivelatore di grandi dimensioni

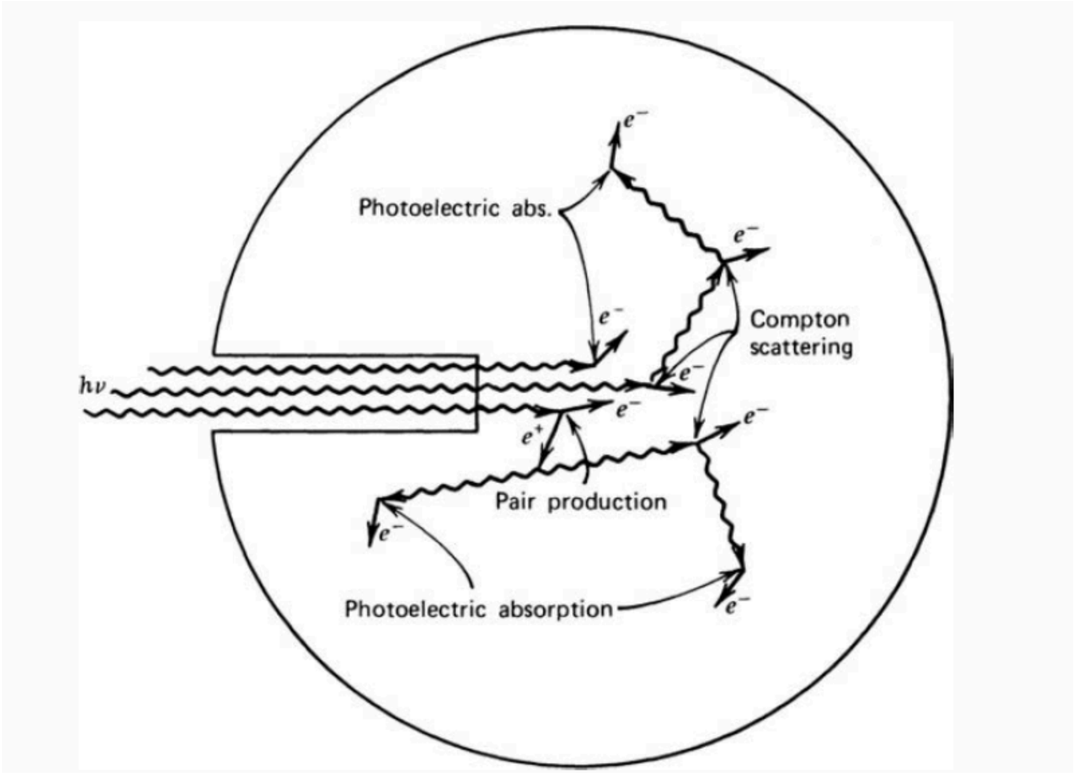

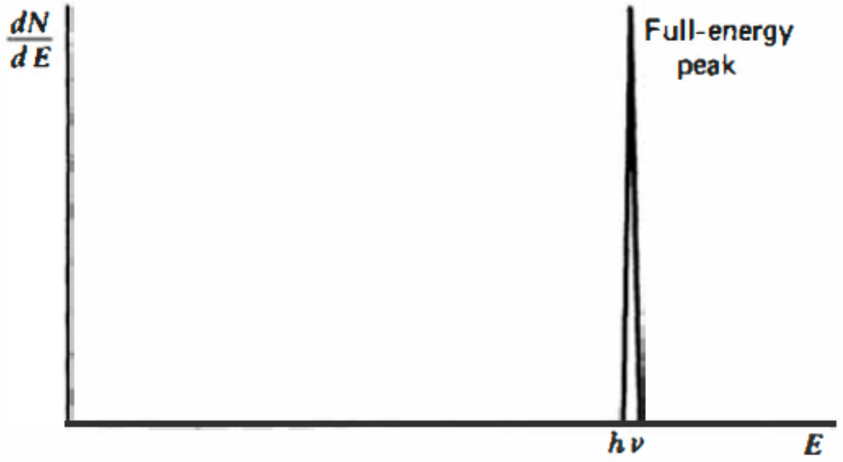

Rivelatore di piccole dimensioni

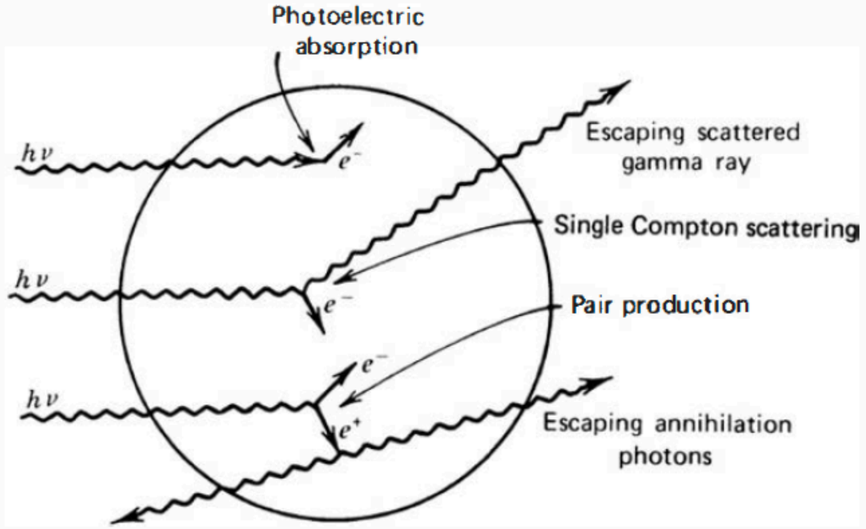

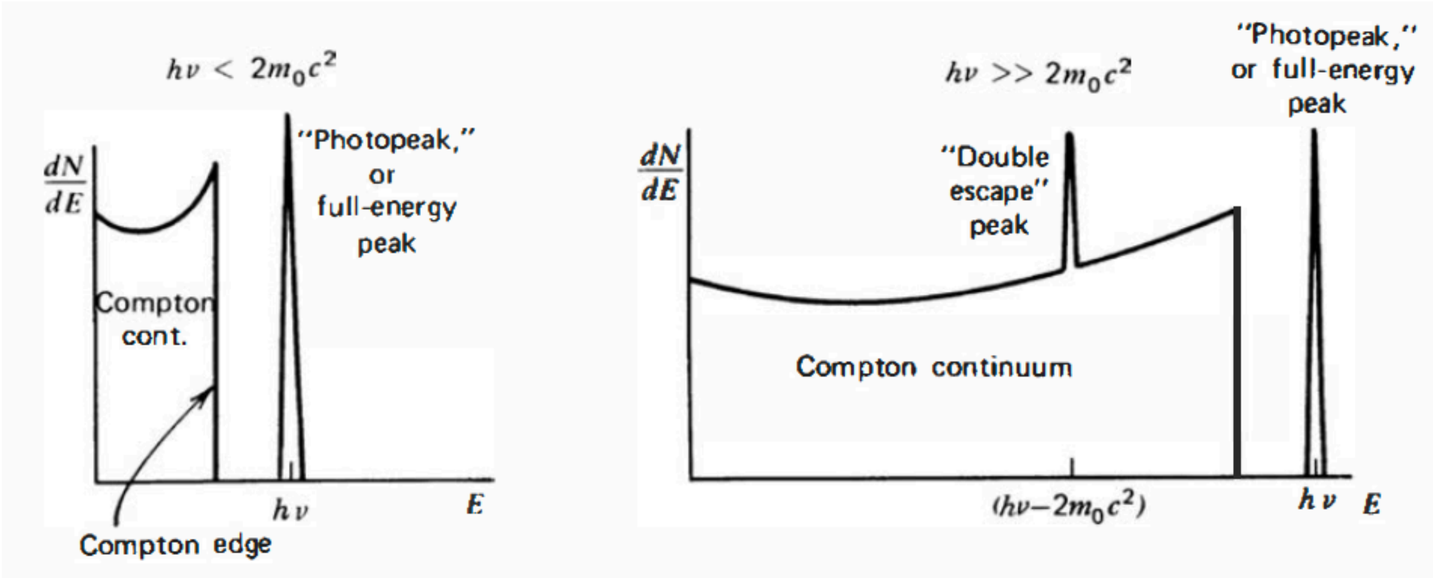

Rivelatore di dimensioni intermedie

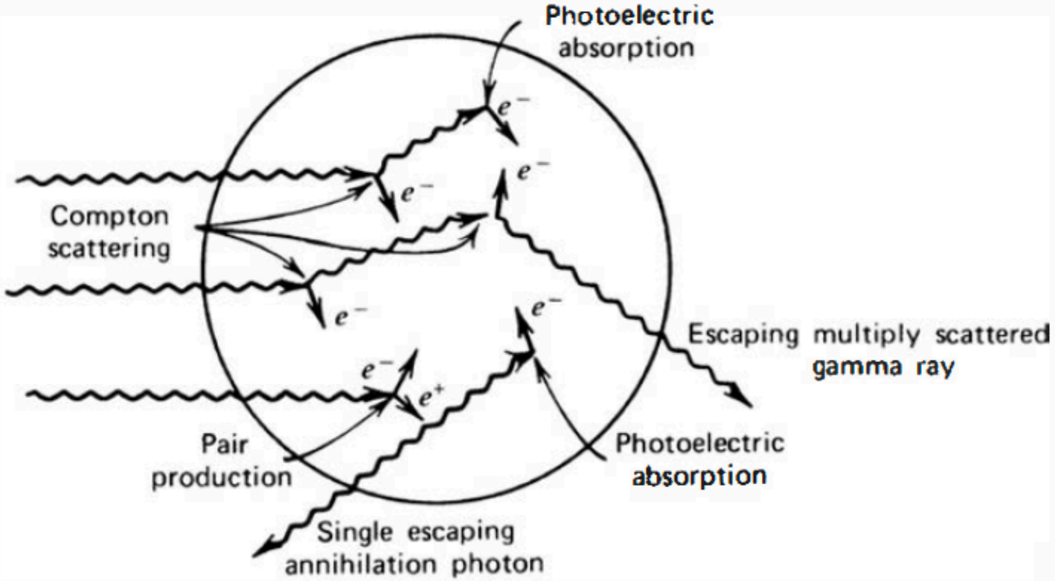

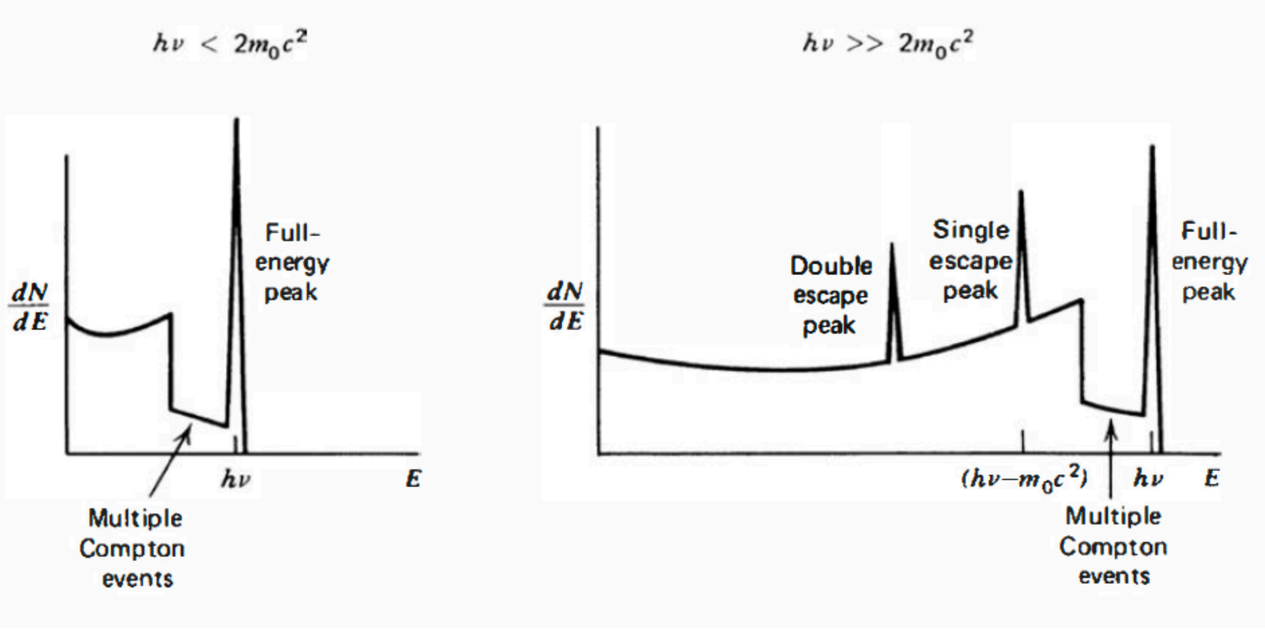

Complicazioni negli spettri “reali”

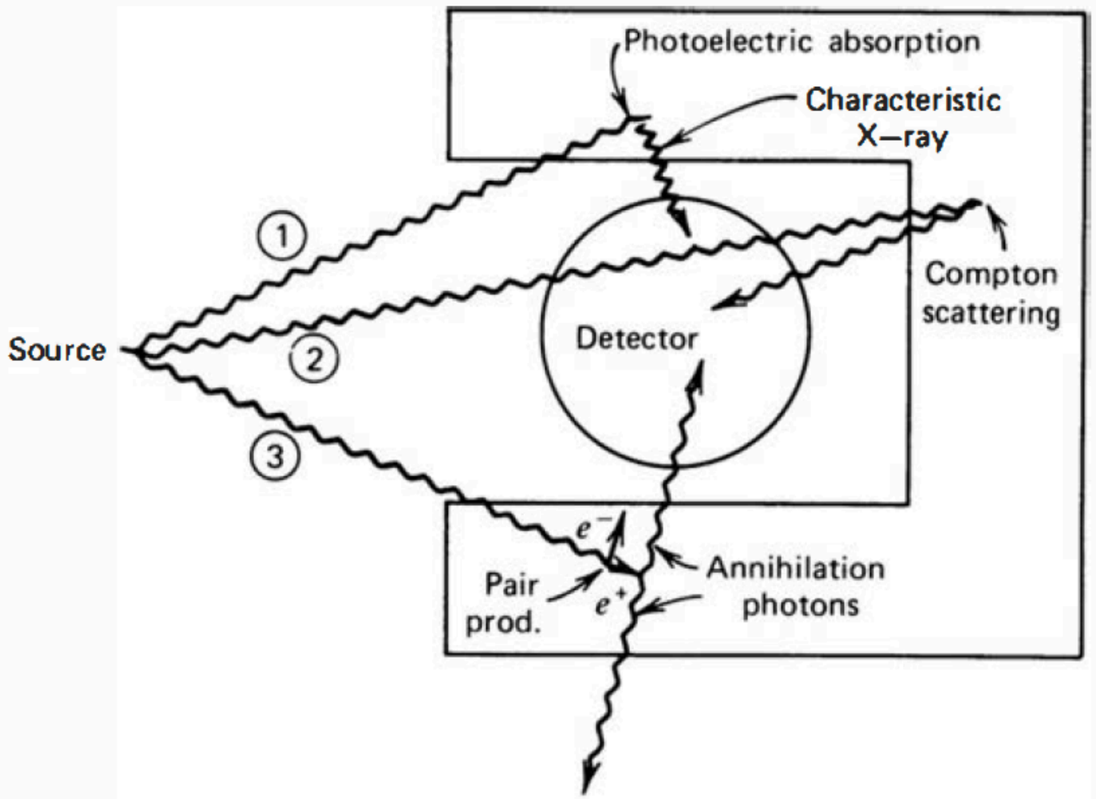

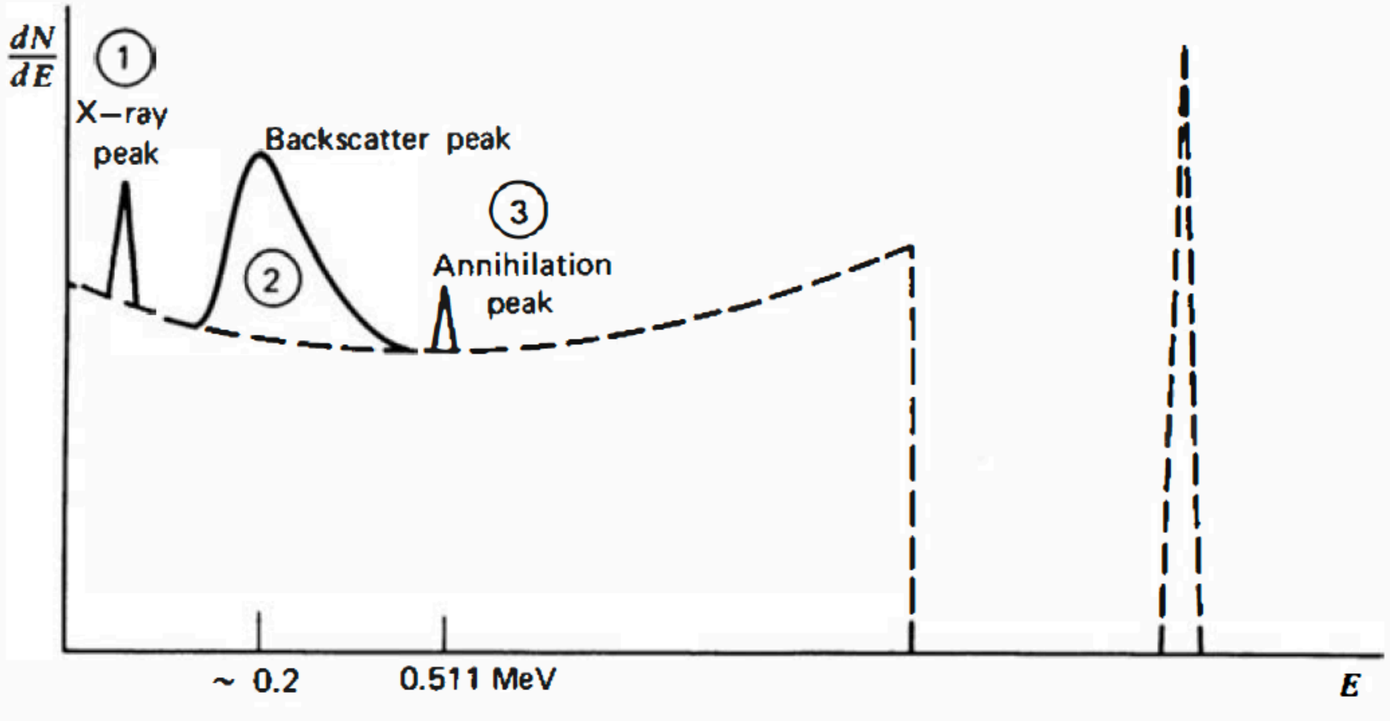

Complicazioni negli spettri "reali"

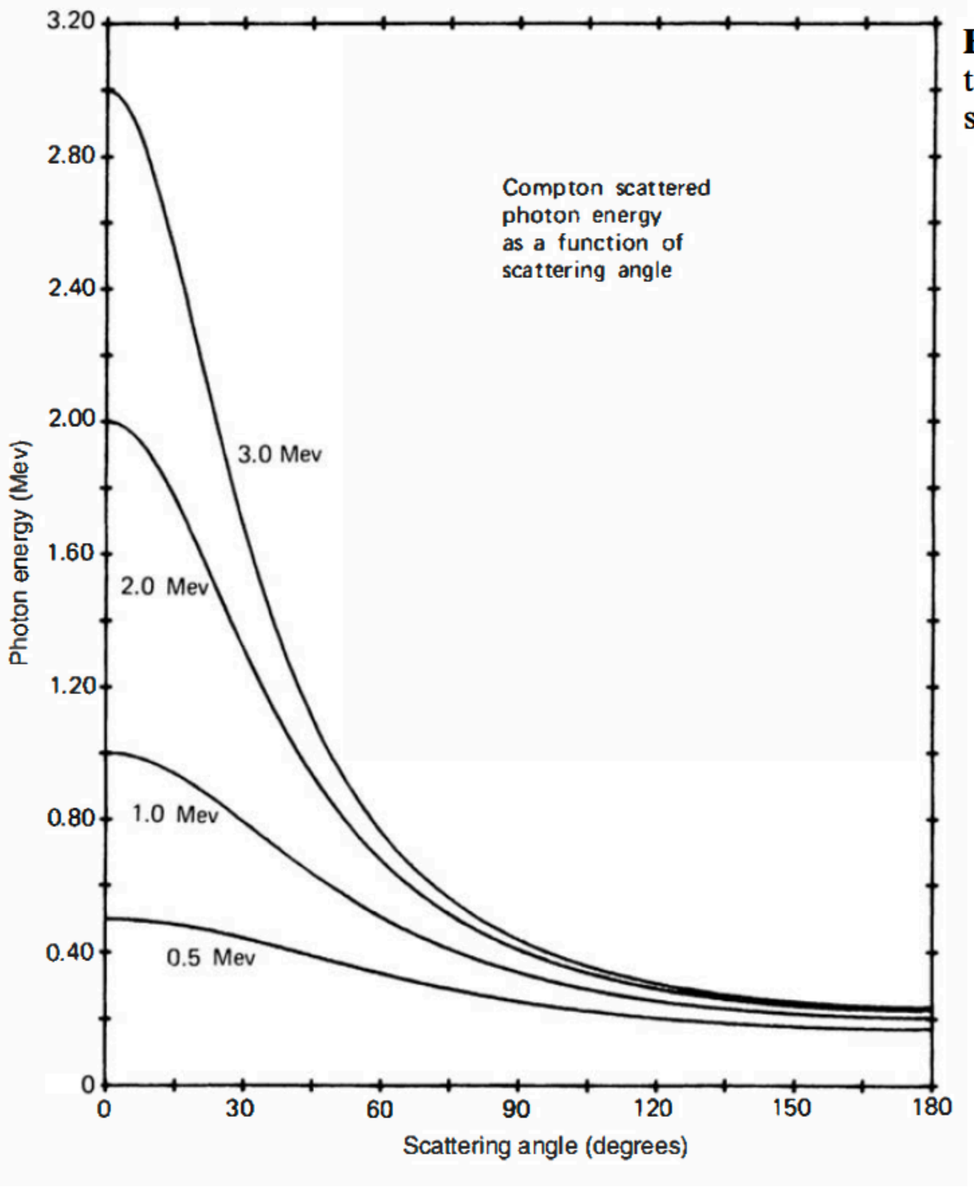

Figure 10.7 Variation of scattered gamma-ray energy with scattering angle.

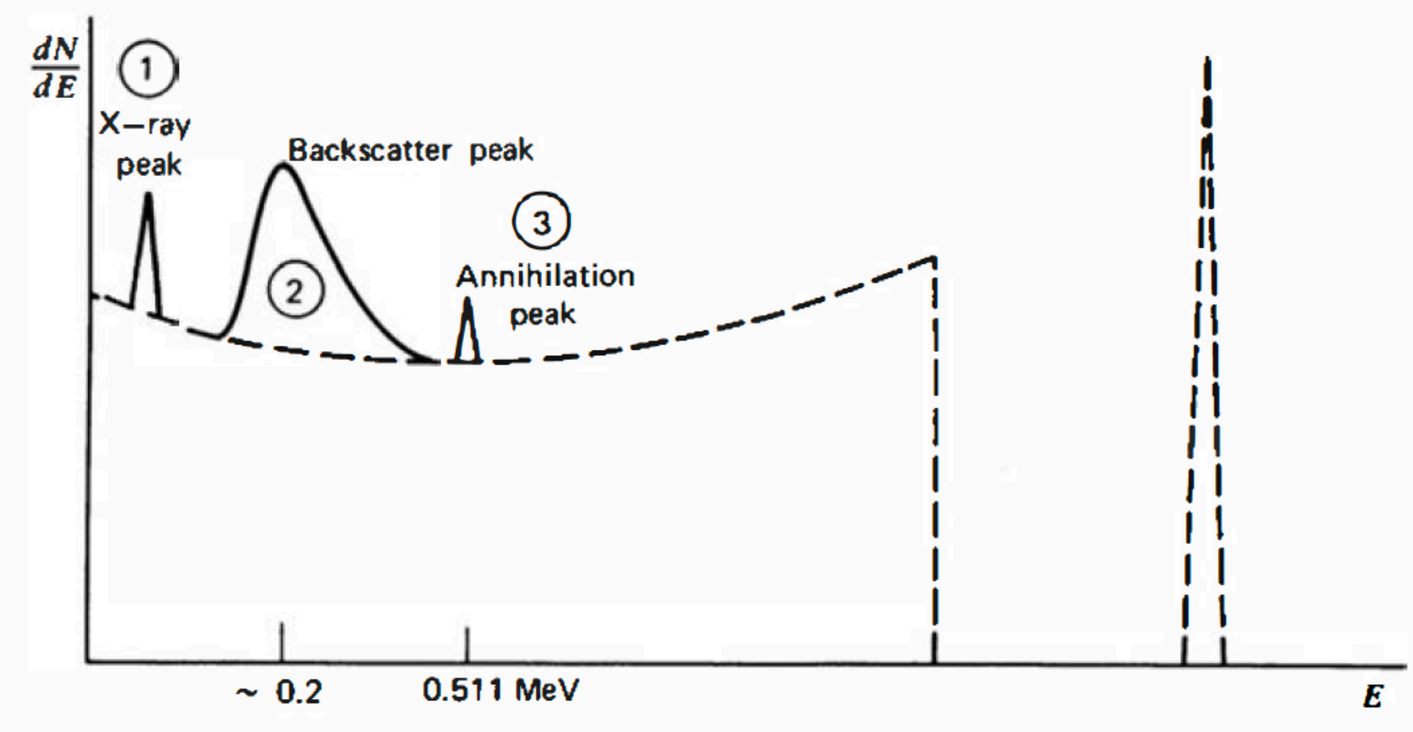

Complicazioni negli spettri “reali”

- “Escape” di elettroni secondari
- “Escape” della radiazione di Bremsstrahlung
- “Escape” di raggi X caratteristici:

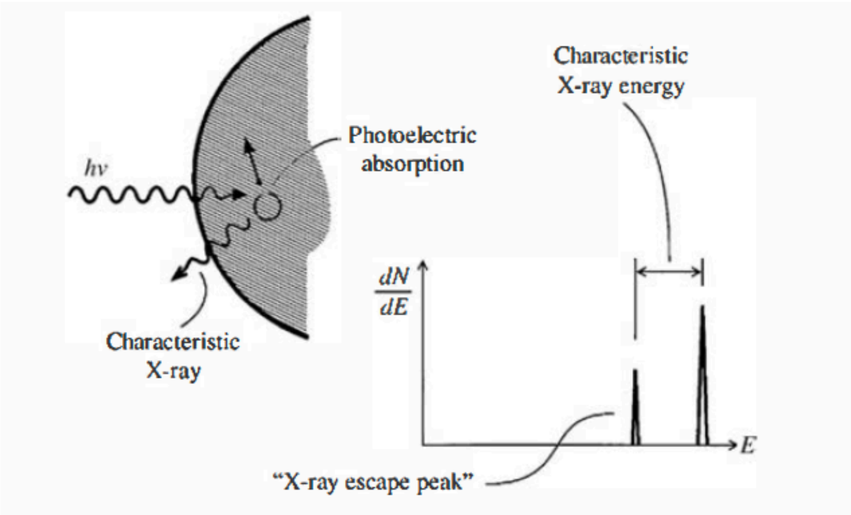

La risoluzione energetica

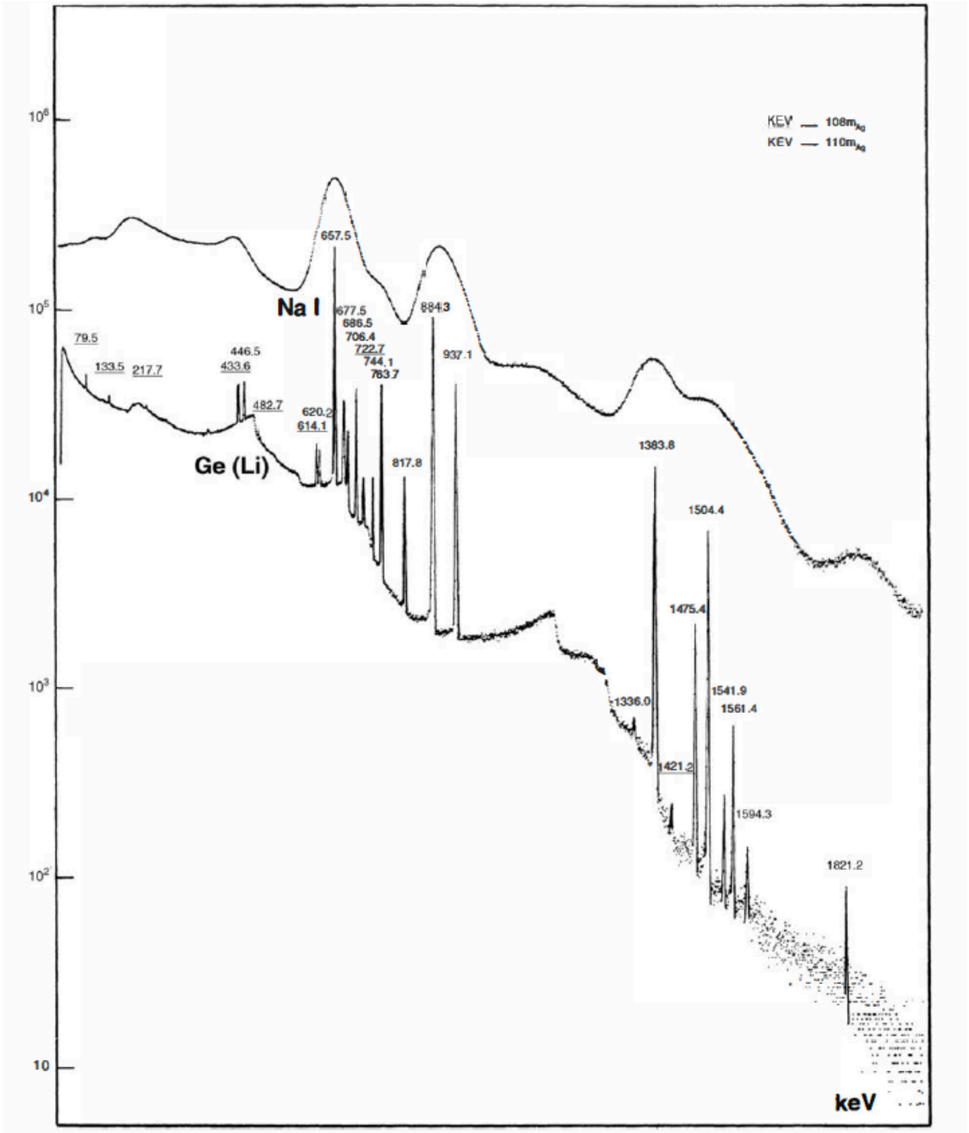

Figure 12.8 Comparative pulse height spectra recorded using a sodium iodide scintillator and a Ge(Li) detector. The source was gamma radiation from the decay of ^{108m}Ag and ^{110m}Ag. Energies of peaks are labeled in keV. (From Philippot.[13])

La risoluzione energetica

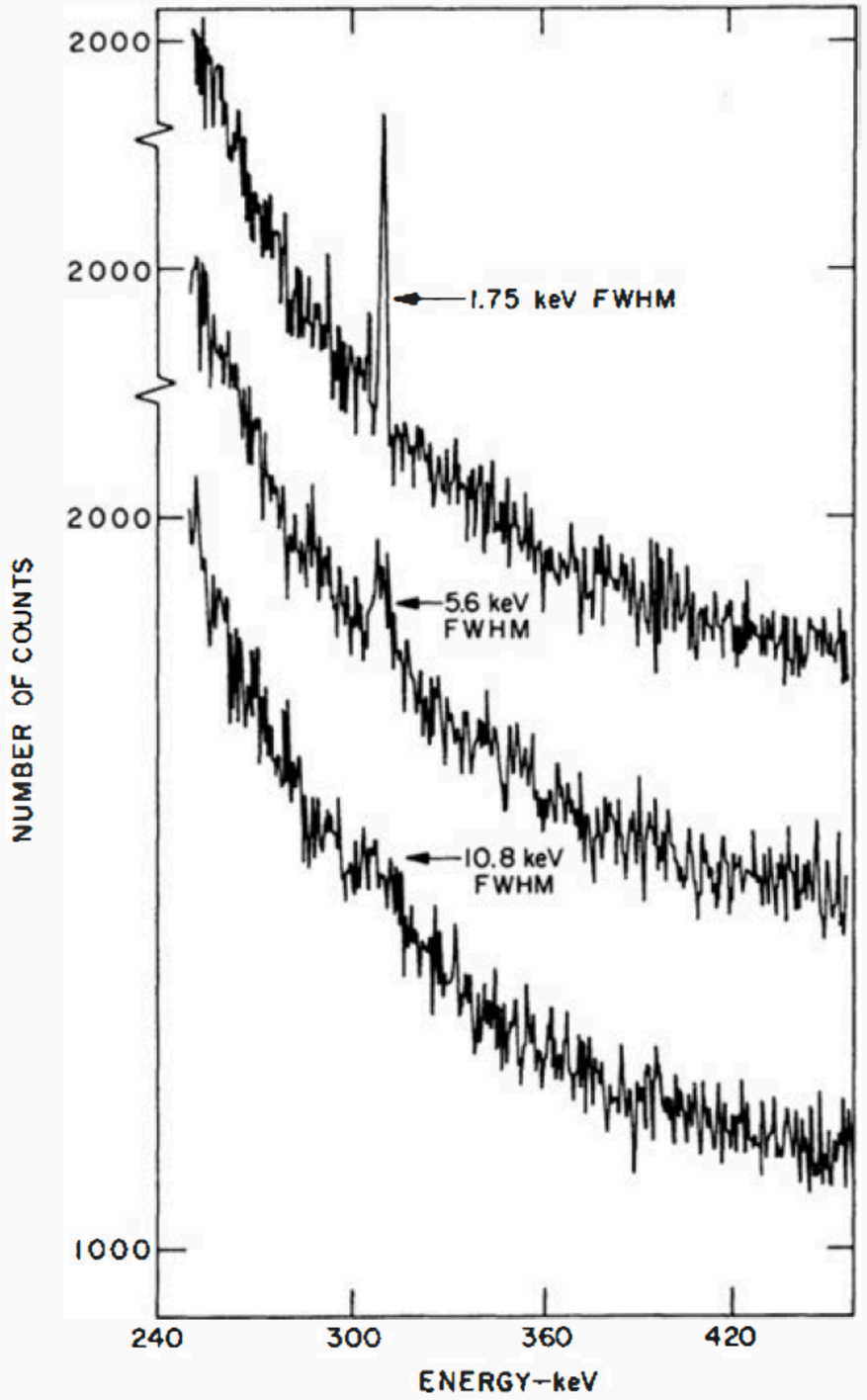

Figure 12.15 The effect of energy resolution on the ability to identify a weak peak superimposed on a statistically uncertain continuum. The area under the peak is the same in all three cases. (From Armantrout et al.[53])

La risoluzione temporale

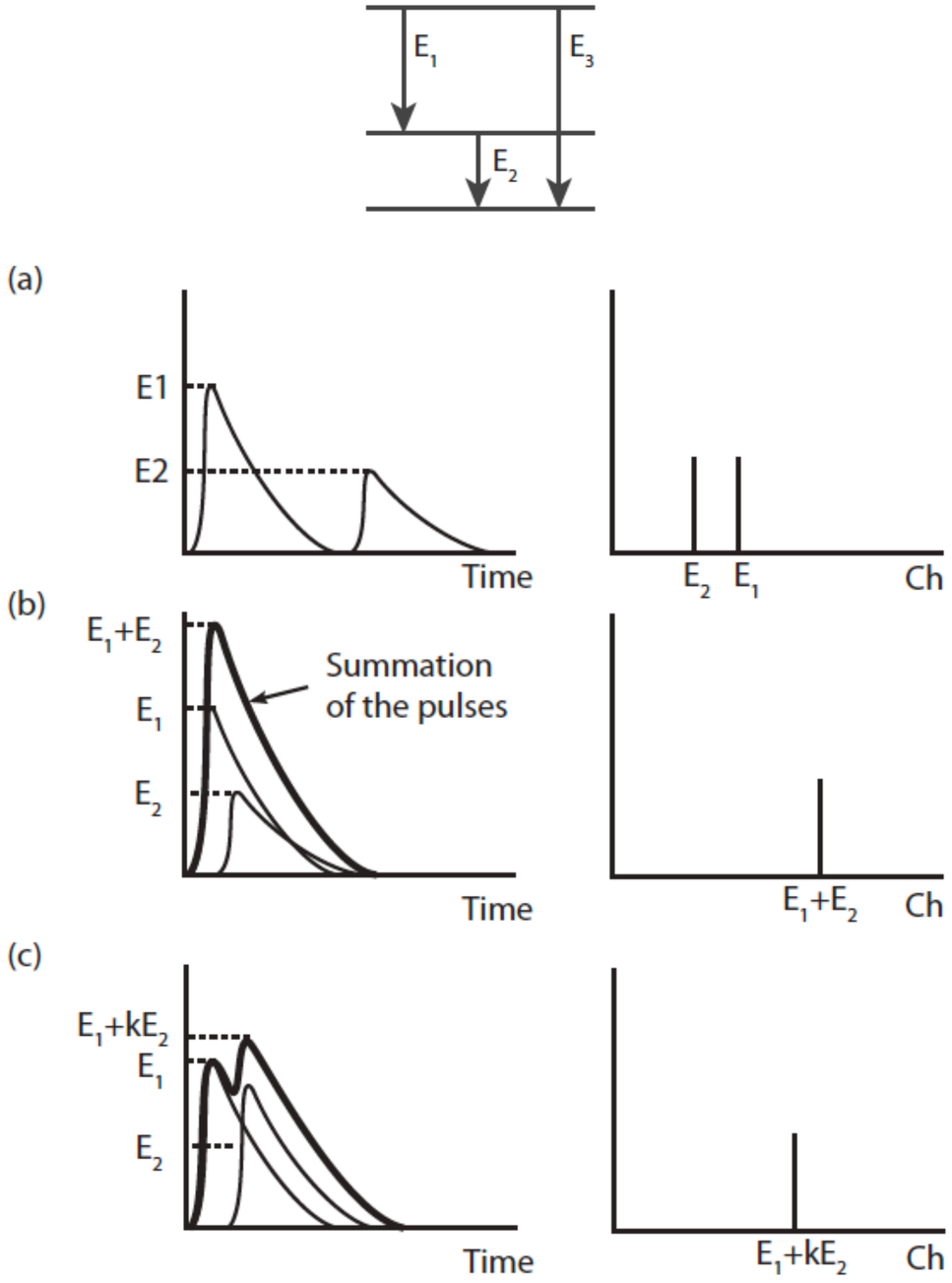

FIGURE 4.51 Top: Principal decay scheme of a γ-ray-emitting radionuclide with two photon energies, E_1 and E_2, respectively. (a) Preamplifier signal and the resulting pulse height distribution from two events, caused by the successive decay of the γ-ray-emitting radionuclide, being registered separately. (b) Preamplifier signal and the resulting pulse height distribution when the two events are both completely registered as one during the pulse rise time, causing a distinct peak located at E_3 (E_1+E_2). (c) Preamplifier signal and the resulting pulse height distribution when the second event is partially causing a count being registered in the interval between E_1 and E_1+E_2.

Esempi di spettri: ^{137}Cs con HPGe

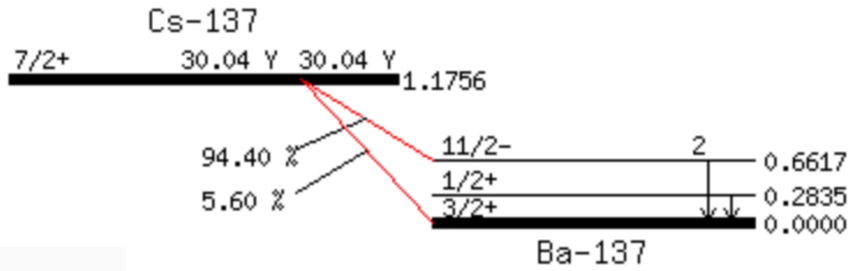

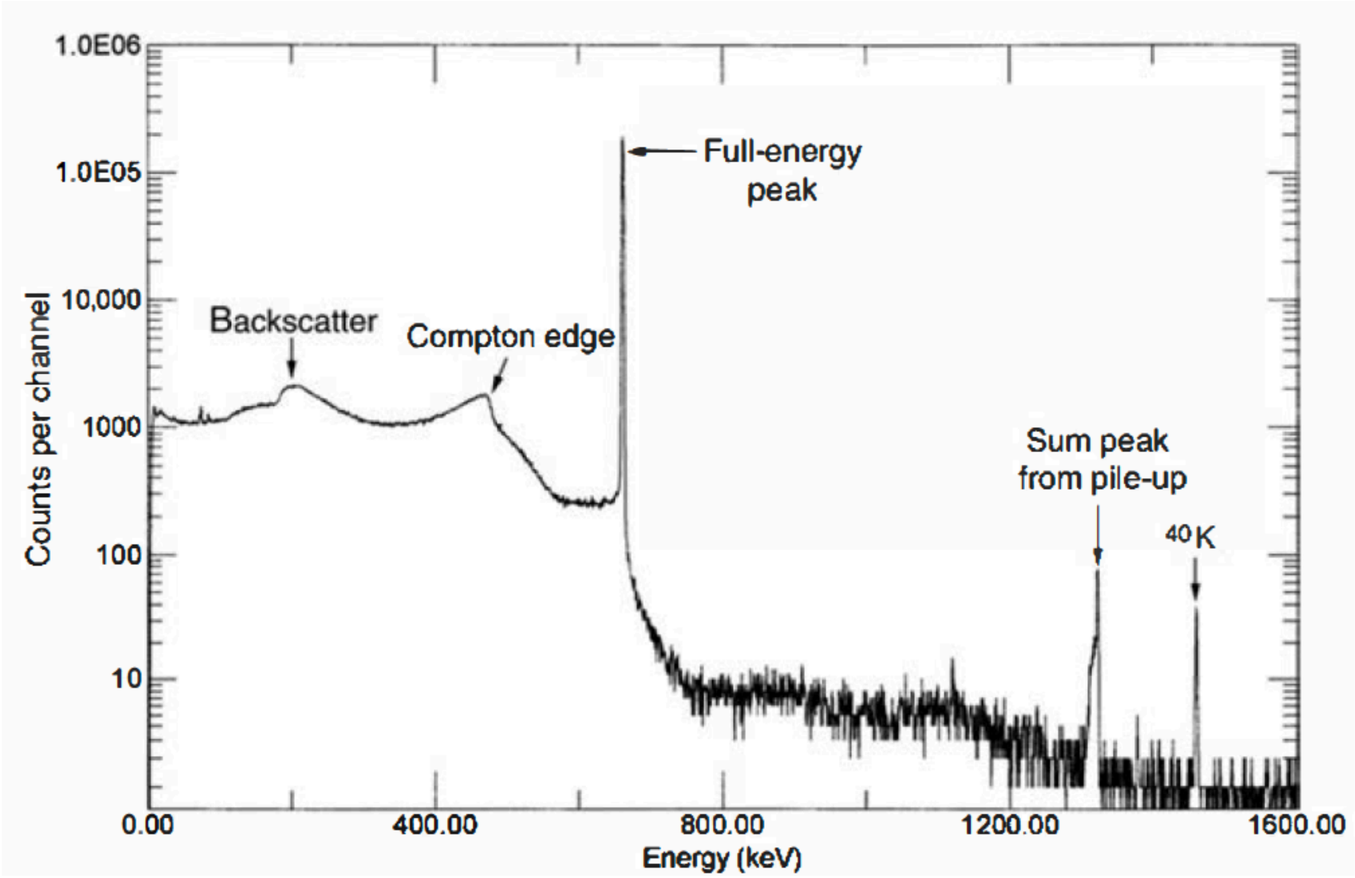

Esempi di spettri: ^{60}Co con HPGe

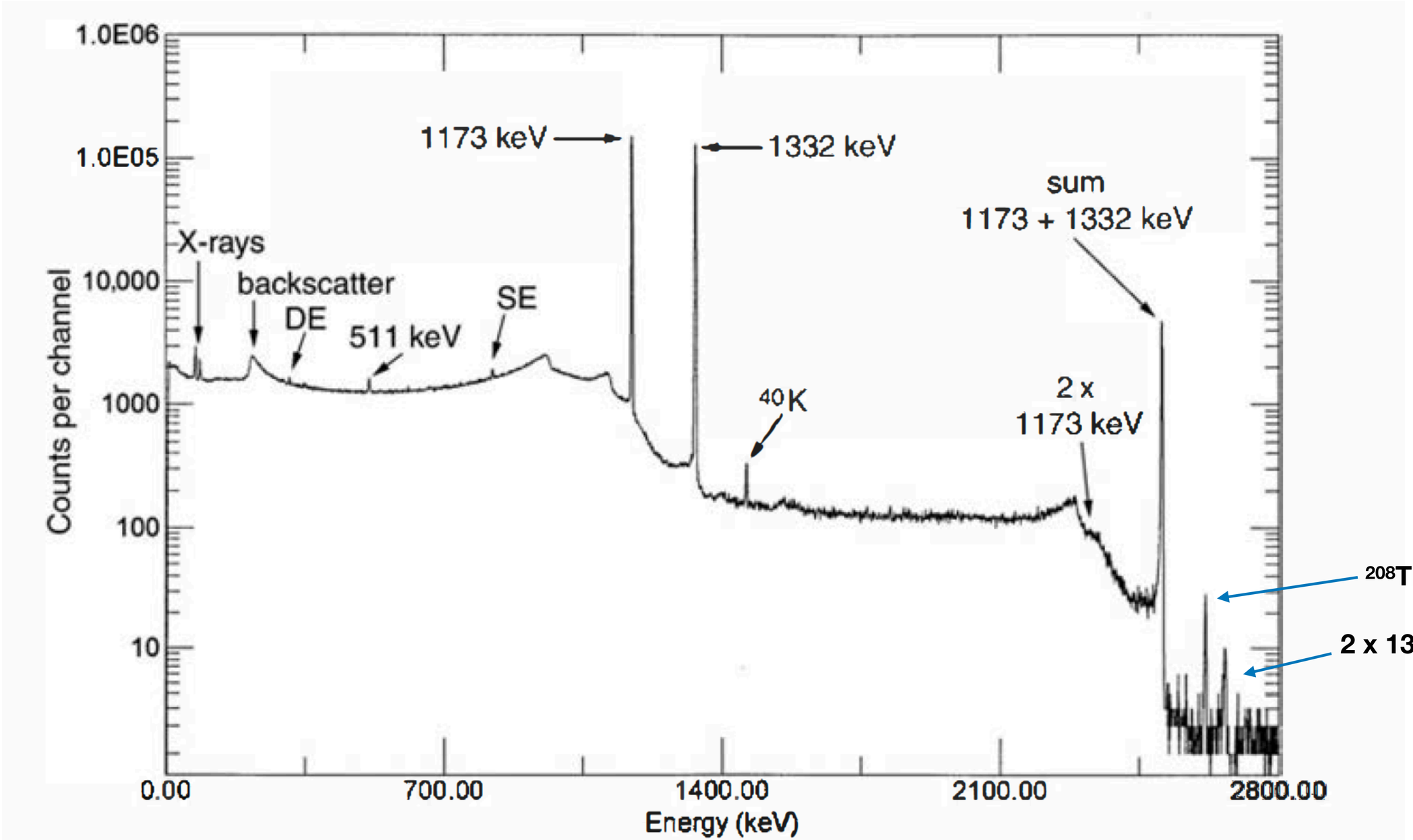

Effetto dell'efficienza relativa su spettri della medesima sorgente di ^{60}Co

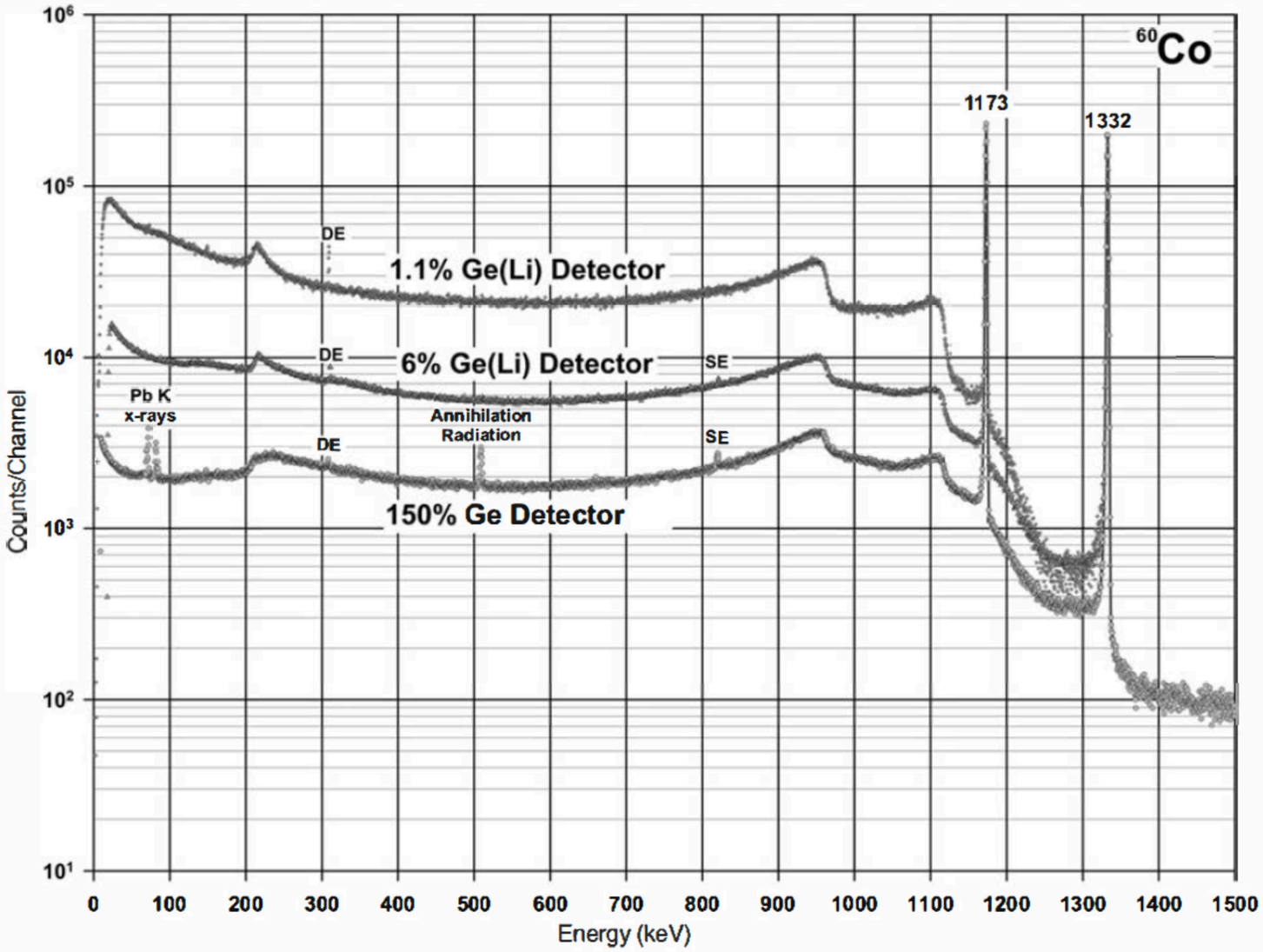

Figure 12.22 ^{60}Co gamma-ray spectra from germanium detectors of three different sizes with the relative efficiencies shown. The plots have been normalized to the same area of the upper full-energy peak. Notice the relative decrease in the importance of the Compton continuum as the detector volume (and efficiency) increases. Note also that the vertical scale is logarithmic, so that the escape peaks are actually somewhat less intense for the largest detector, even though they are quite evident because of the lower Compton continuum on which they are superimposed. (From Helmer et al.[62])

Esempi di spettri: ^{24}Na con HPGe

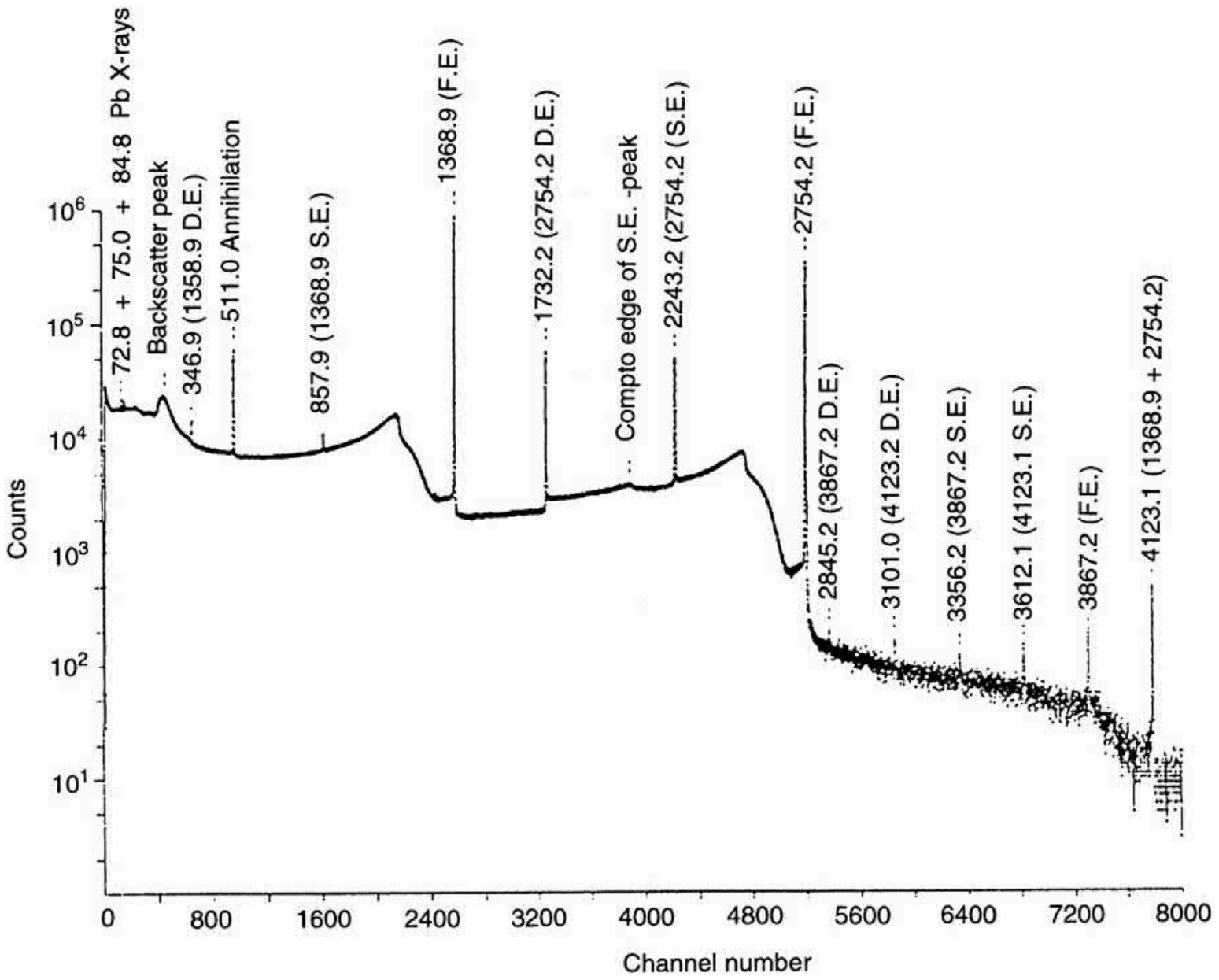

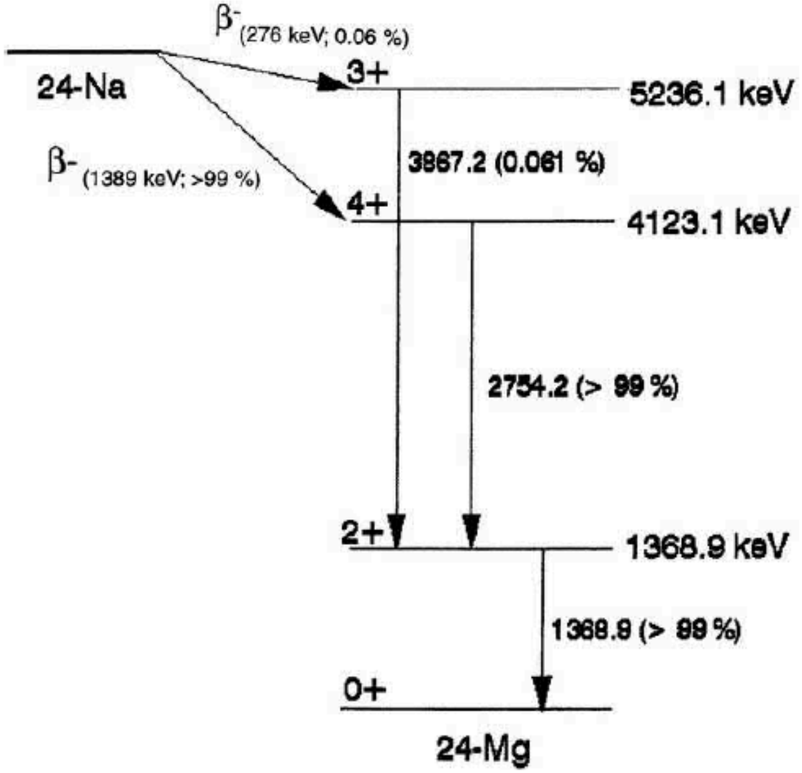

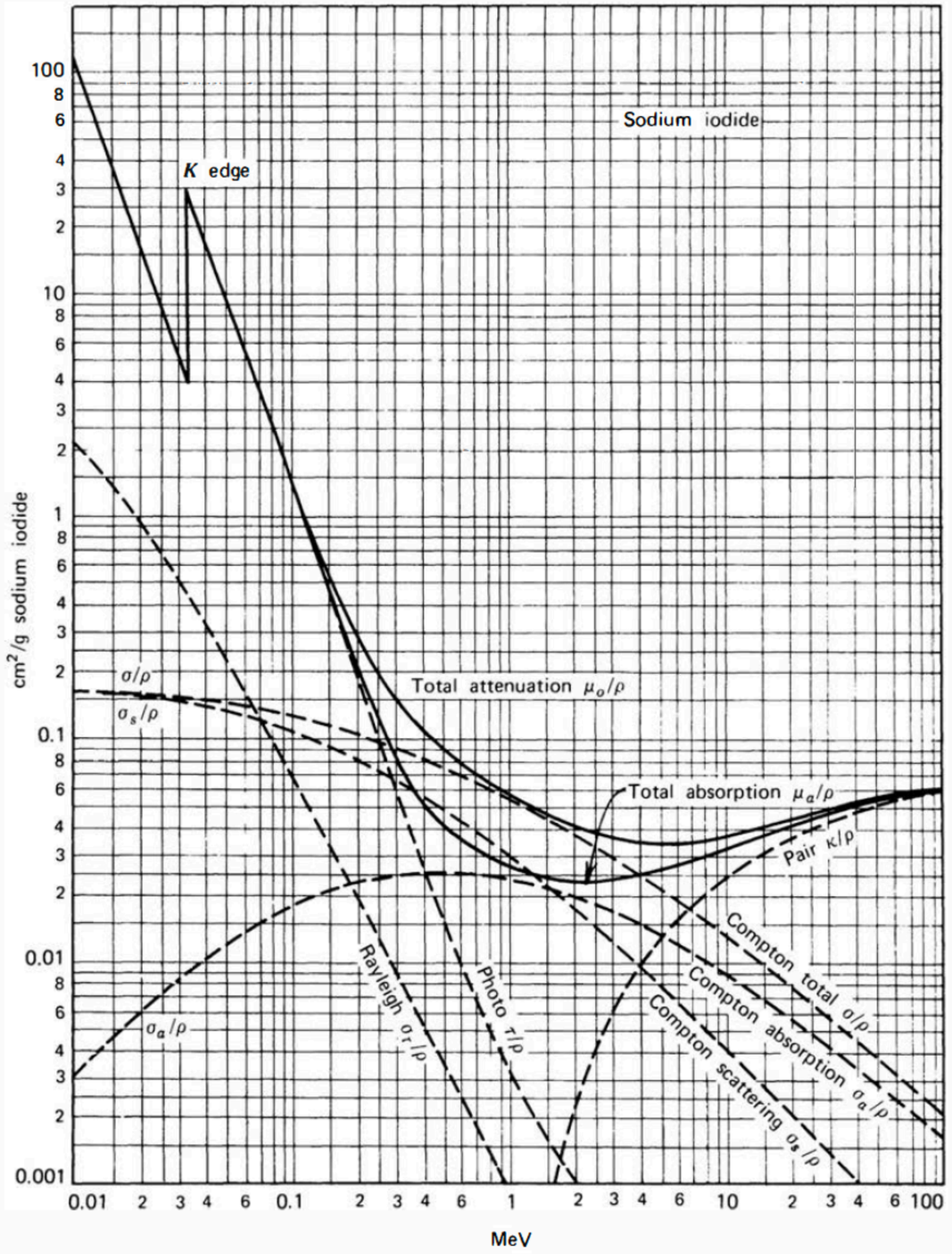
Sodium iodide
K edge
Total attenuation μ_o/ρ
Total absorption μ_a/ρ
σ/ρ
σ_s/ρ
σ_a/ρ
Pair κ/ρ
Compton total σ/ρ
Compton absorption σ_a/ρ
Compton scattering σ_s/ρ
Rayleigh σ_r/ρ
Photo τ/ρ
cm^2/g sodium iodide
MeV

Germanium

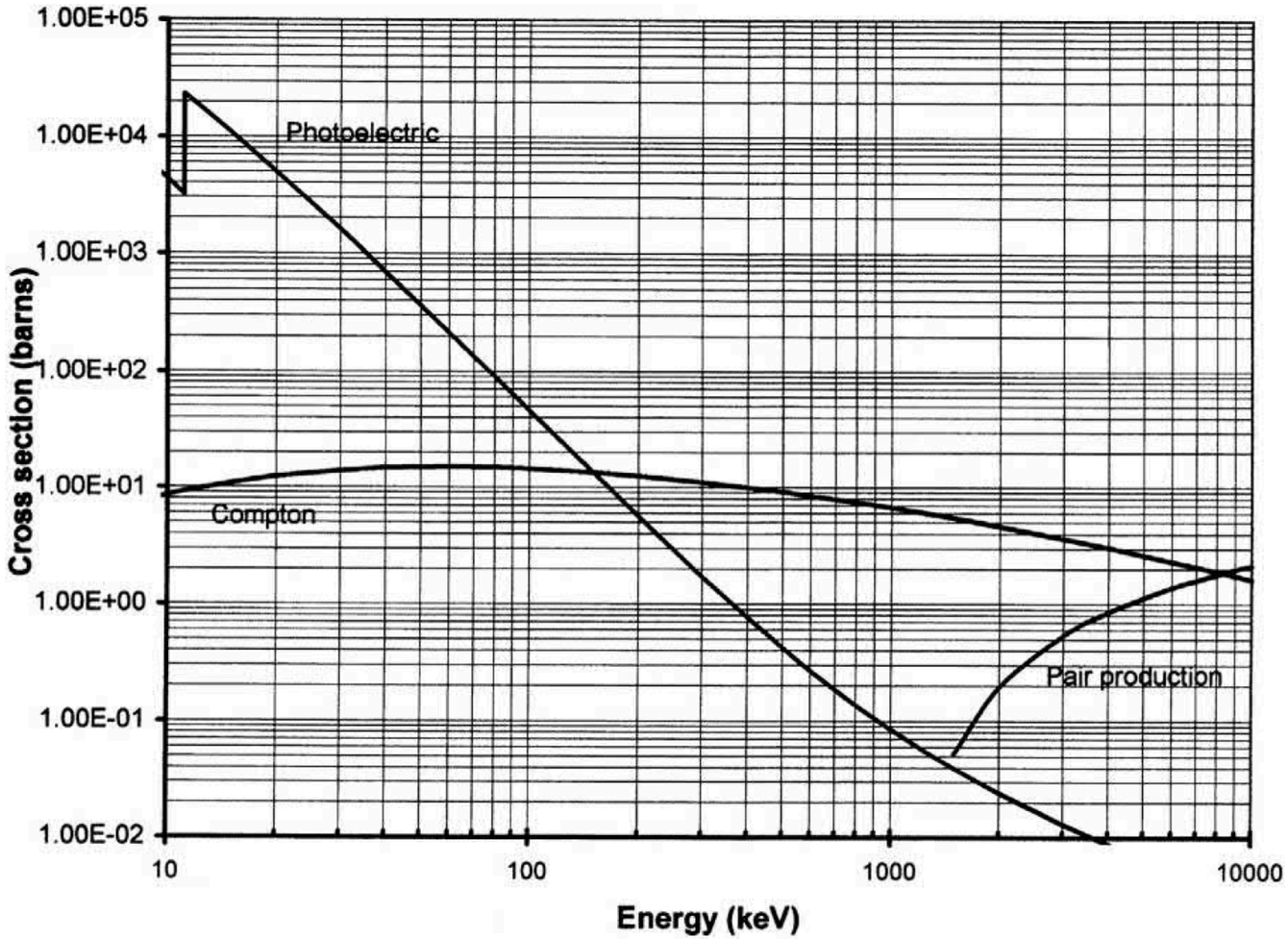
Photoelectric
Compton
Pair production
Cross section (barns)
Energy (keV)

Semiconduttori

Table 11.1 Properties of Intrinsic Silicon and Germanium

	Si	Ge
Atomic number	14	32
Atomic weight	28.09	72.60
Stable isotope mass numbers	28-29-30	70-72-73-74-76
Density (300 K); g/cm^3	2.33	5.32
Atoms/cm^3	4.96×10^{22}	4.41×10^{22}
Dielectric constant (relative to vacuum)	12	16
Forbidden energy gap (300 K); eV	1.115	0.665
Forbidden energy gap (0 K); eV	1.165	0.746
Intrinsic carrier density (300 K); cm^{-3}	1.5×10^{10}	2.4×10^{13}
Intrinsic resistivity (300 K); $\Omega \cdot cm$	2.3×10^5	47
Electron mobility (300 K); $cm^2/V \cdot s$	1350	3900
Hole mobility (300 K); $cm^2/V \cdot s$	480	1900
Electron mobility (77 K); $cm^2/V \cdot s$	2.1×10^4	3.6×10^4
Hole mobility (77 K); $cm^2/V \cdot s$	1.1×10^4	4.2×10^4
Energy per electron–hole pair (300 K); eV	3.62	
Energy per electron–hole pair (77 K); eV	3.76	2.96
Fano factor (77 K)	0.143 (Ref. 7)	0.129 (Ref. 9)
	0.084 (Ref. 8)	0.08 (Ref. 10)
	0.085 to 0.137 (Ref. 12)	< 0.11 (Ref. 11)
		0.057 to 0.064 (Ref. 12)
	0.16 (Ref. 13)	0.058 (Ref. 14)

Source: G. Bertolini and A. Coche (eds.), *Semiconductor Detectors*, Elsevier-North Holland, Amsterdam, 1968, except where noted.

Configurazione operativa di un rivelatore HPGe

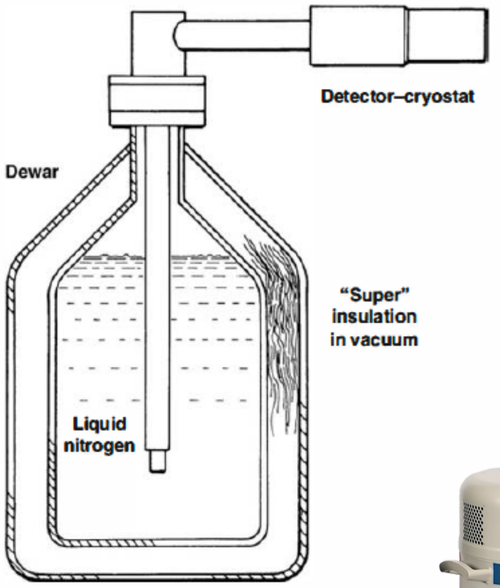

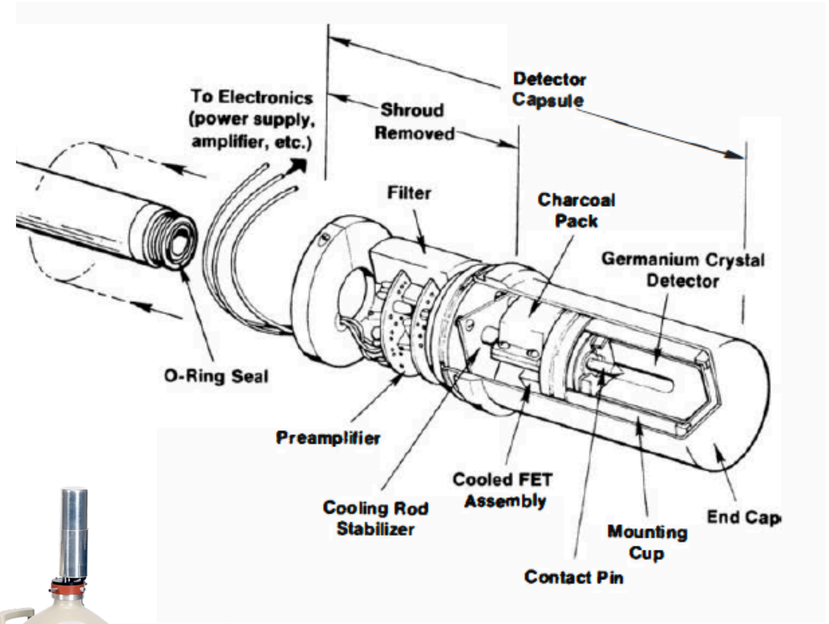

HPGe Coassiale

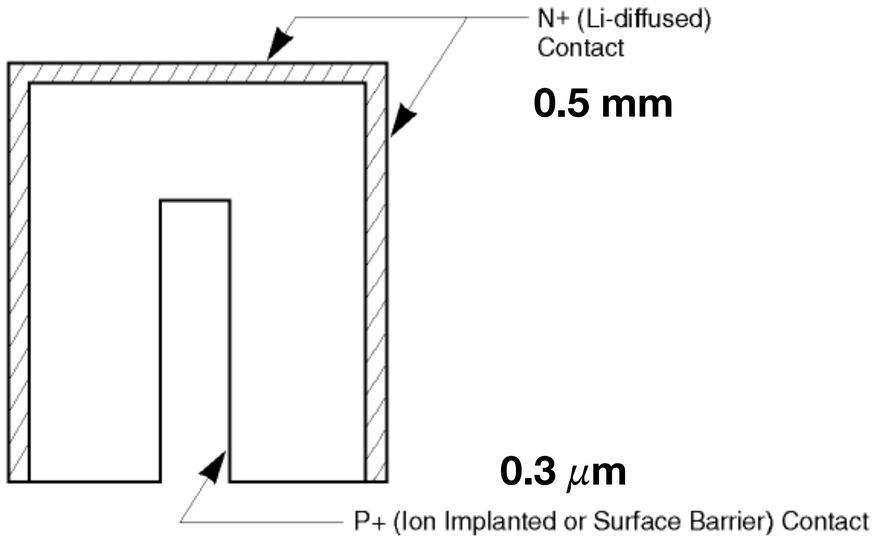

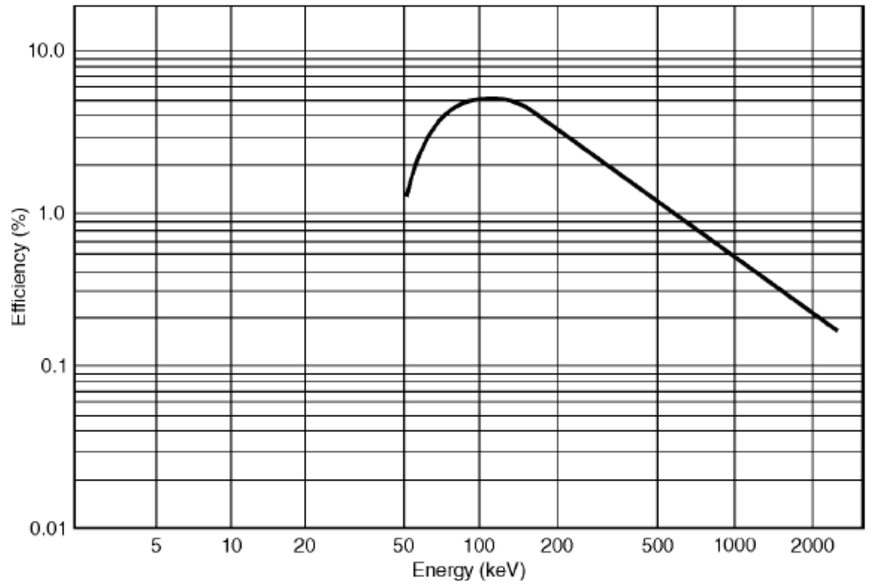

0.5 mm Al end-cap

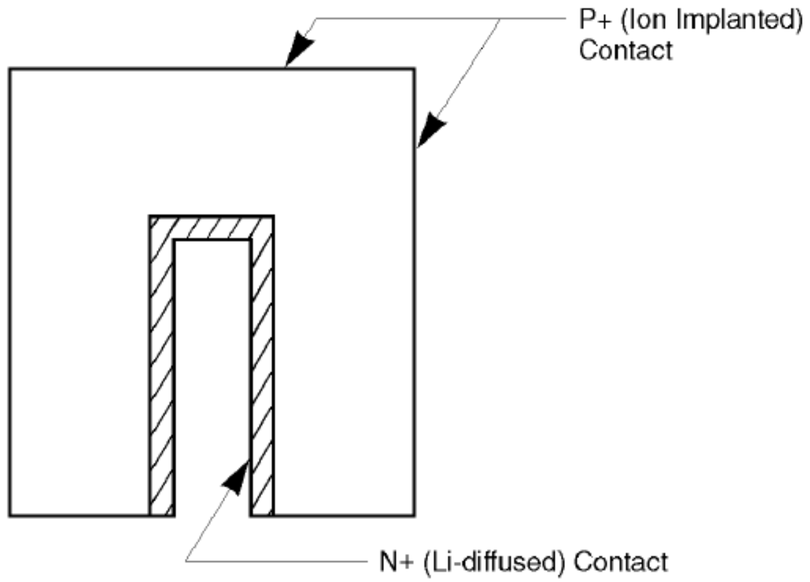

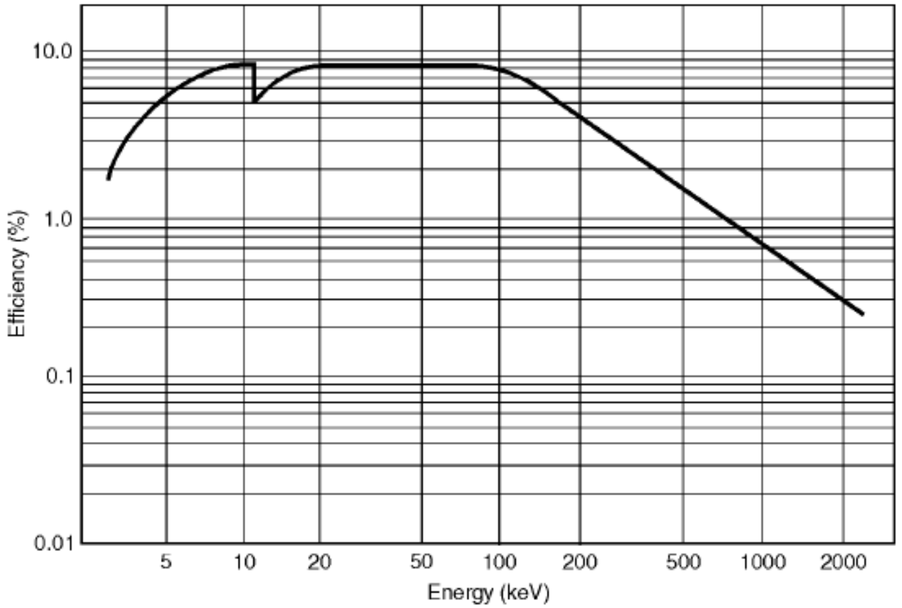

0.6 mm finestra carbonio

HPGe Well type (a pozzetto)

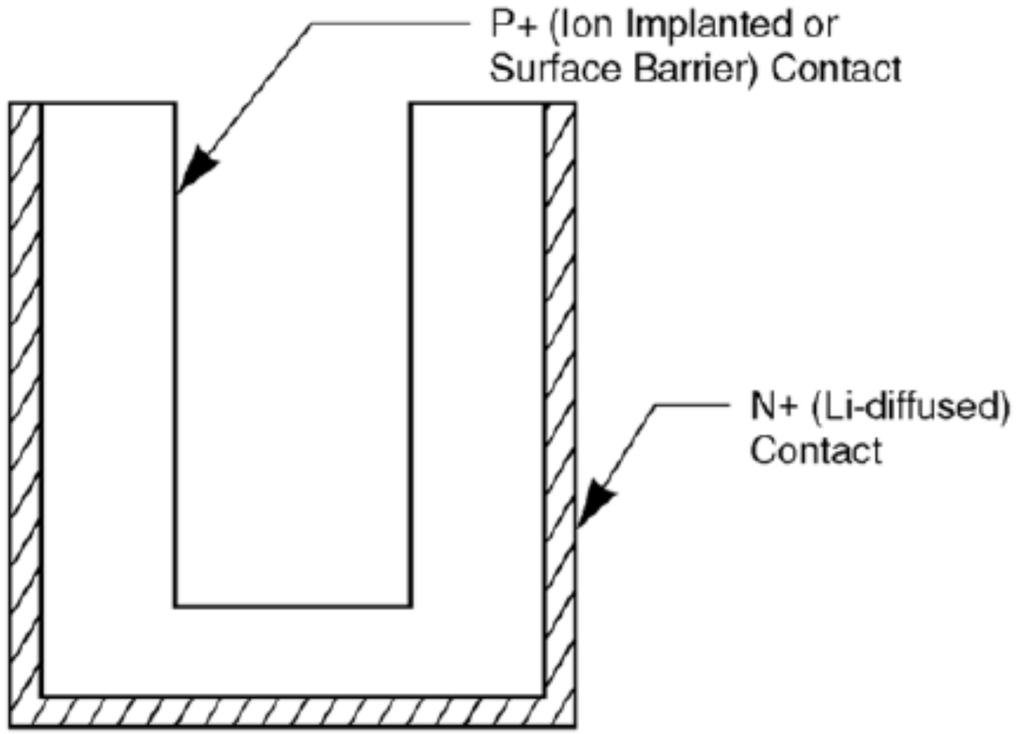

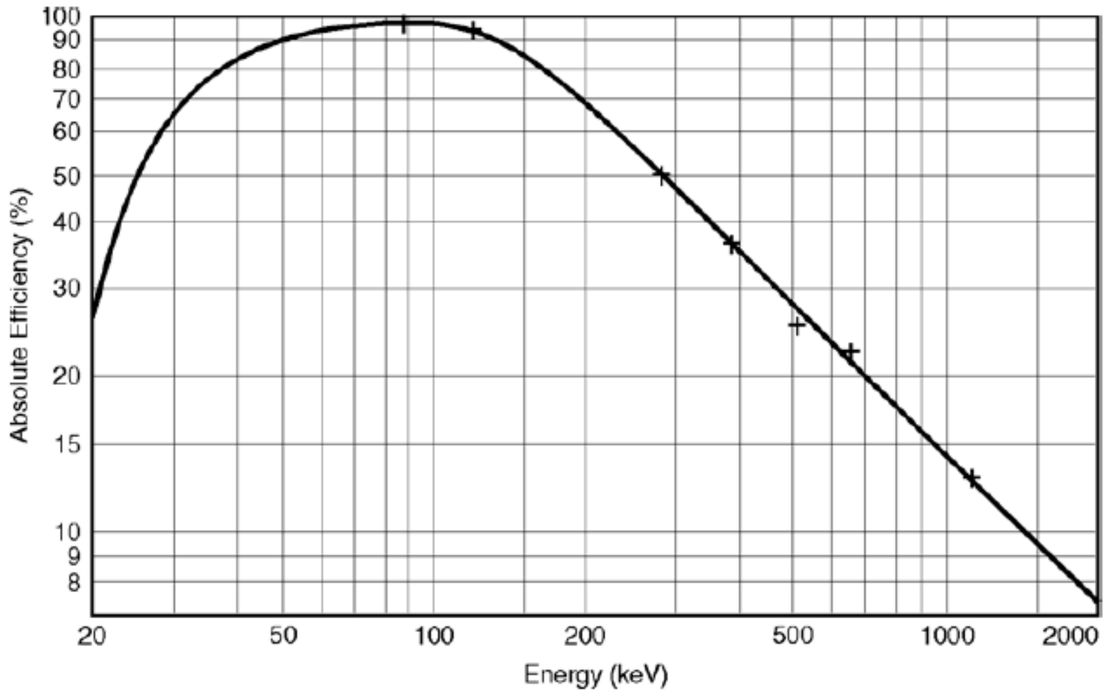

0.5 mm Al end-cap

HPGe Mirion Technologies

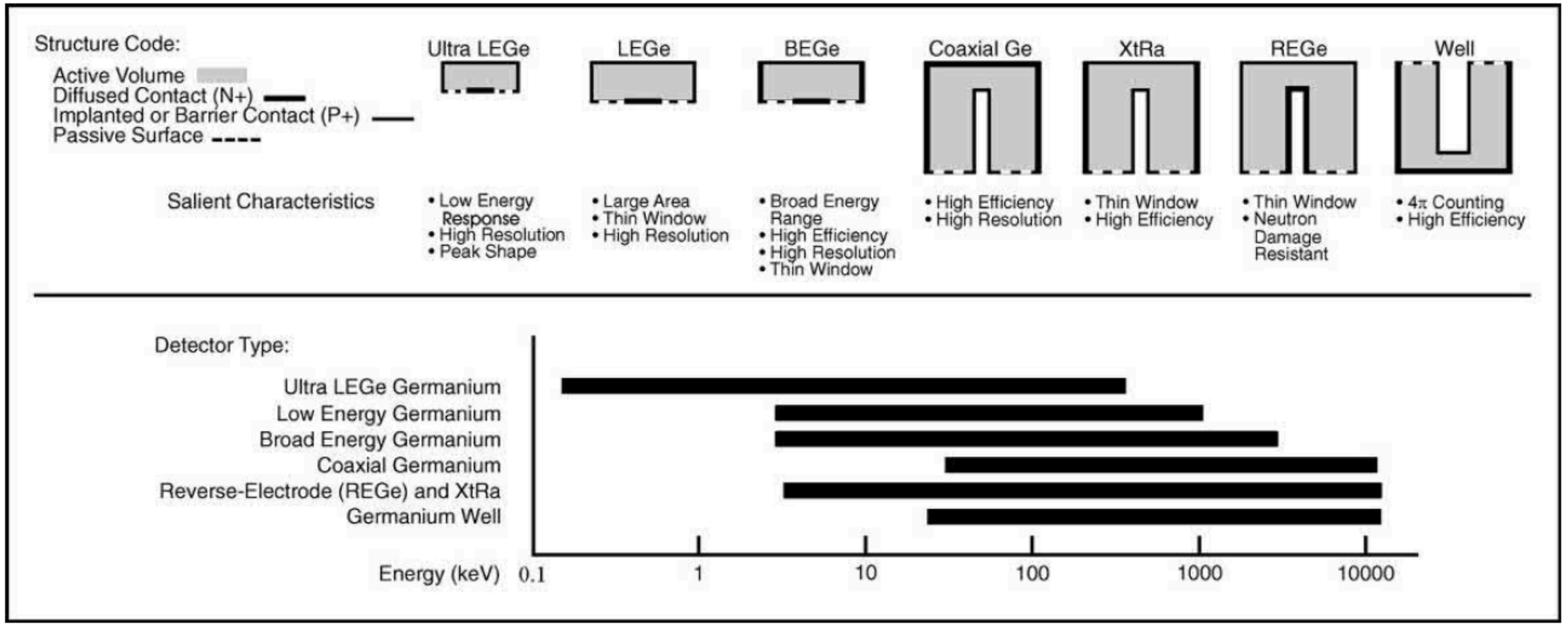

Variazione dell'efficienza intrinseca

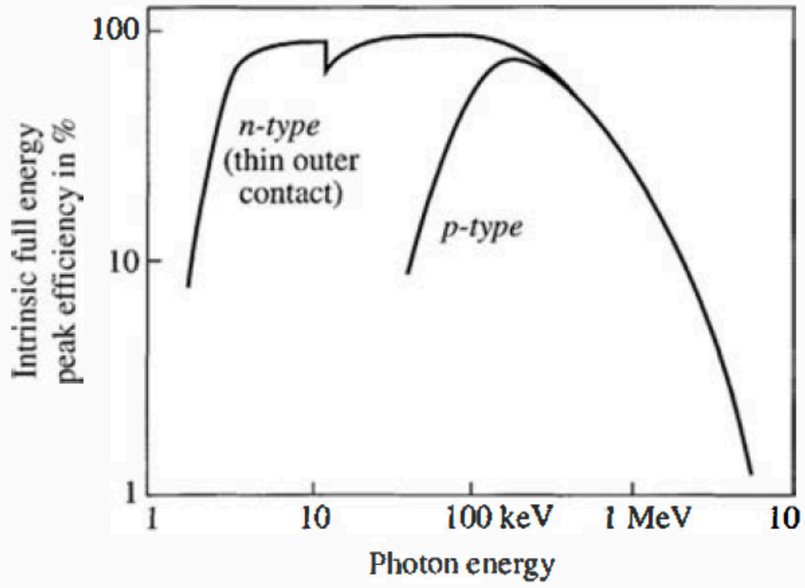

Figure 12.31 General character of the variation of intrinsic peak efficiency for coaxial germanium detectors with incident photon energy. The difference between *n*- and *p*-type detector behavior at low energies is caused by the attenuation due to different contact thicknesses.

Variazione dell'efficienza intrinseca

FIGURE 4.16 Superposition of two efficiency curves for the same low-energy detector mounted with two different endcaps: 0.15 mm Be (upper curve) and 0.5 mm Al (lower curve). The source-to-detector distance was 5 cm. The curves are polynomial fits through the experimental points.

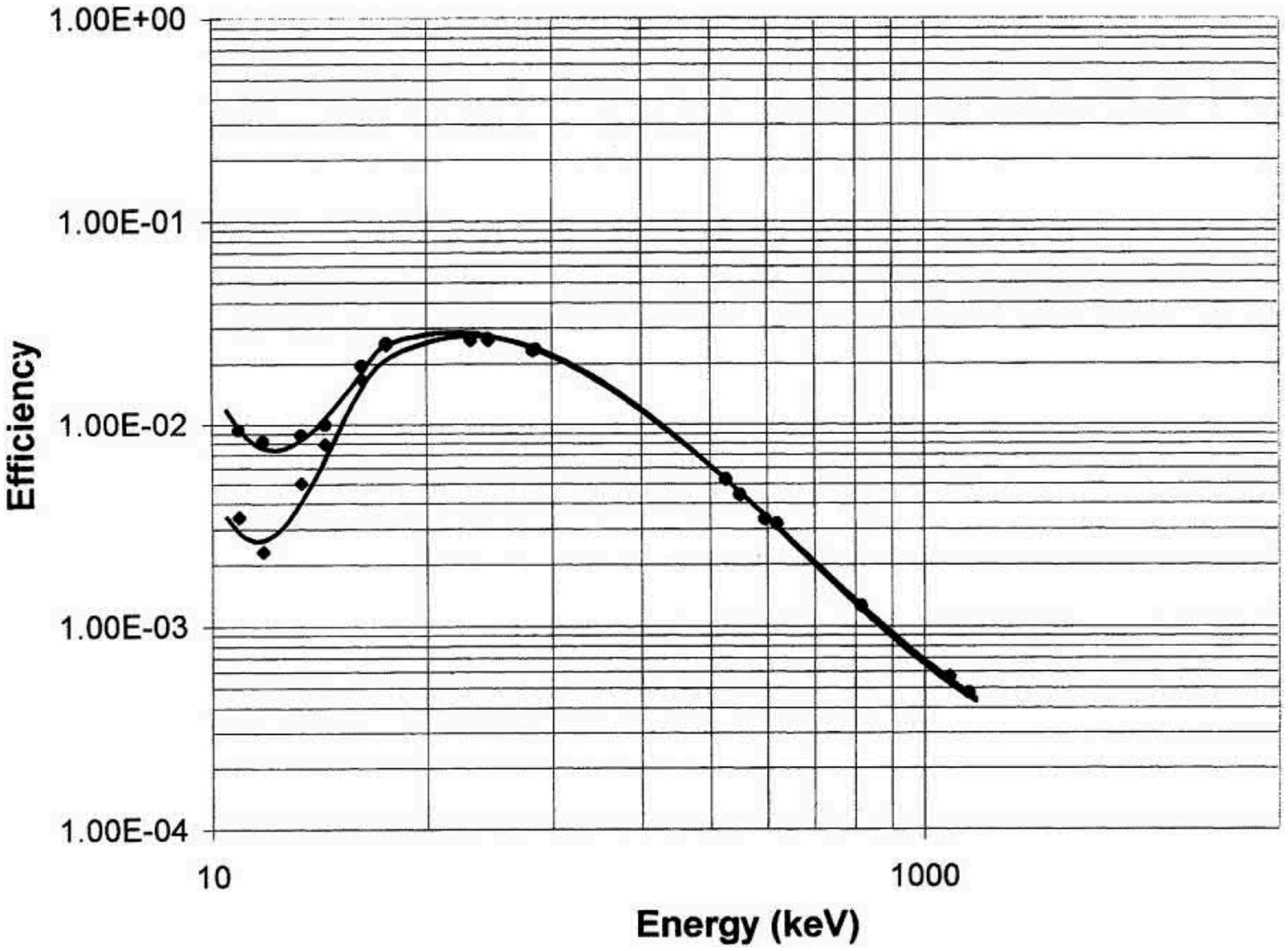

Attenuazione γ in Ge

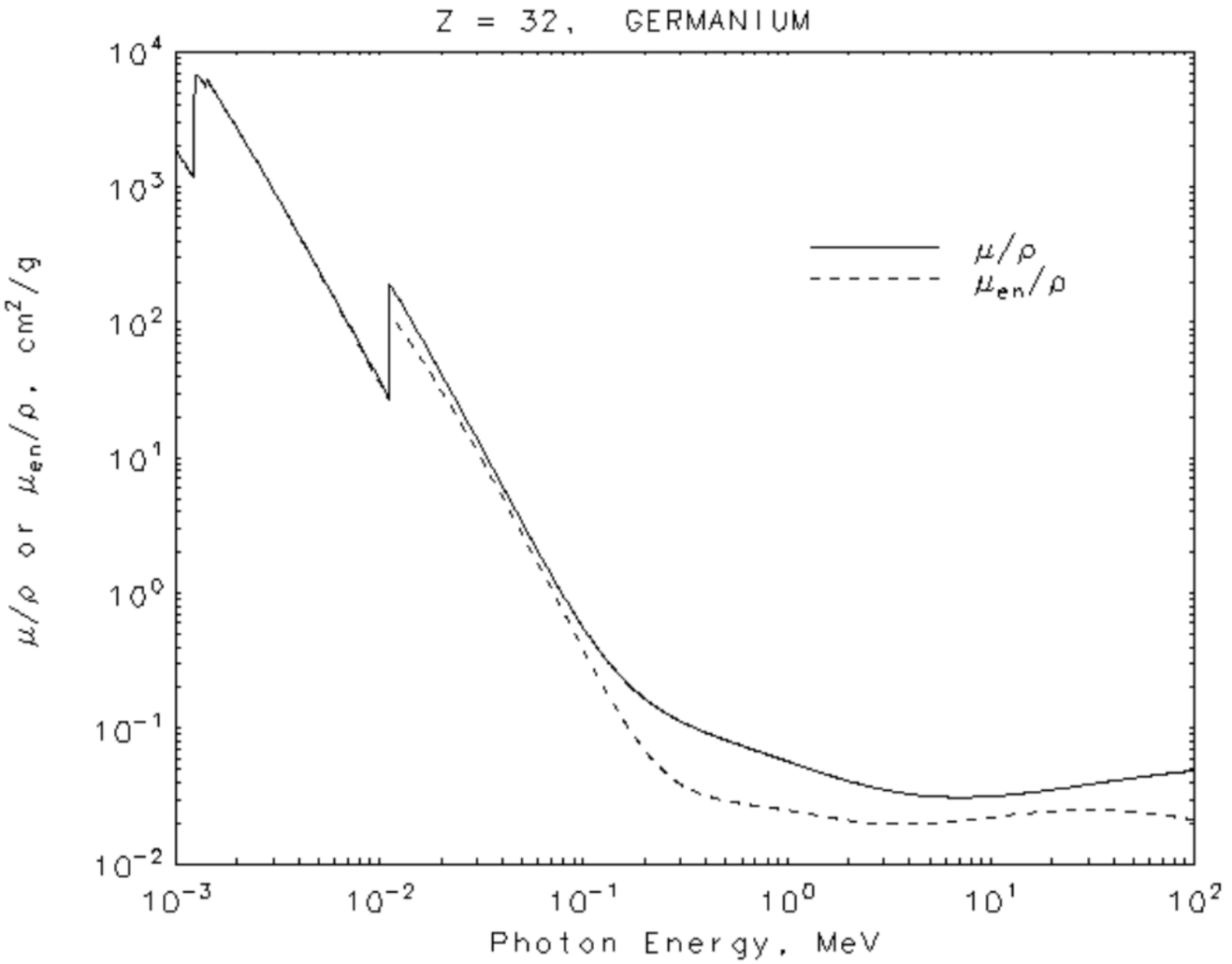

	Energy (MeV)	μ/ρ (cm²/g)	μ_{en}/ρ (cm²/g)
	1.00000E-03	1.893E+03	1.887E+03
	1.10304E-03	1.502E+03	1.496E+03
	1.21670E-03	1.190E+03	1.185E+03
L3	1.21670E-03	4.389E+03	4.343E+03
	1.23215E-03	4.734E+03	4.684E+03
	1.24780E-03	4.974E+03	4.922E+03
L2	1.24780E-03	6.698E+03	6.622E+03
	1.32844E-03	6.348E+03	6.279E+03
	1.41430E-03	5.554E+03	5.495E+03
L1	1.41430E-03	6.287E+03	6.221E+03
	1.50000E-03	5.475E+03	5.420E+03
	2.00000E-03	2.711E+03	2.688E+03
	3.00000E-03	9.613E+02	9.527E+02
	4.00000E-03	4.497E+02	4.445E+02
	5.00000E-03	2.472E+02	2.433E+02
	6.00000E-03	1.509E+02	1.477E+02
	8.00000E-03	6.890E+01	6.660E+01
	1.00000E-02	3.742E+01	3.564E+01
	1.11031E-02	2.811E+01	2.653E+01
K	1.11031E-02	1.981E+02	1.157E+02
	1.50000E-02	9.152E+01	6.256E+01
	2.00000E-02	4.222E+01	3.178E+01
	3.00000E-02	1.385E+01	1.126E+01
	4.00000E-02	6.207E+00	5.152E+00
	5.00000E-02	3.335E+00	2.759E+00
	6.00000E-02	2.023E+00	1.642E+00
	8.00000E-02	9.501E-01	7.184E-01
	1.00000E-01	5.550E-01	3.803E-01
	1.50000E-01	2.491E-01	1.288E-01
	2.00000E-01	1.661E-01	6.865E-02
	3.00000E-01	1.131E-01	3.891E-02
	4.00000E-01	9.327E-02	3.193E-02
	5.00000E-01	8.212E-02	2.930E-02
	6.00000E-01	7.452E-02	2.790E-02
	8.00000E-01	6.426E-02	2.618E-02
	1.00000E+00	5.727E-02	2.489E-02
	1.25000E+00	5.101E-02	2.353E-02
	1.50000E+00	4.657E-02	2.242E-02
	2.00000E+00	4.086E-02	2.094E-02
	3.00000E+00	3.524E-02	1.977E-02
	4.00000E+00	3.275E-02	1.962E-02
	5.00000E+00	3.158E-02	1.987E-02
	6.00000E+00	3.107E-02	2.027E-02
	8.00000E+00	3.103E-02	2.120E-02
	1.00000E+01	3.156E-02	2.208E-02
	1.50000E+01	3.340E-02	2.364E-02
	2.00000E+01	3.528E-02	2.452E-02

Schermature

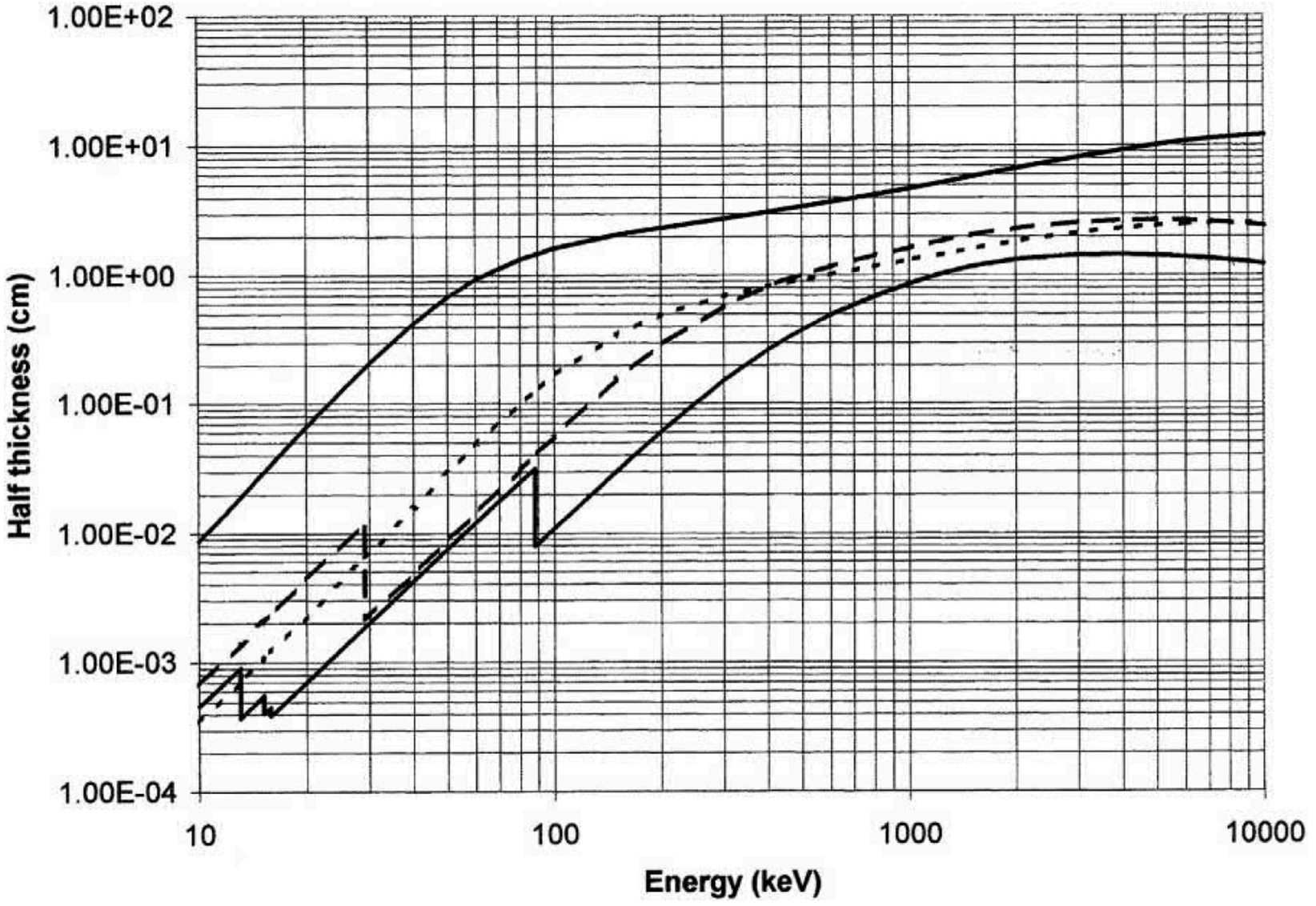

FIGURE 4.18 Half-thickness in centimeter for Pb (lower plain curve), Sn (dashed curve), Cu (dotted curve), and Si (upper plain curve) as a function of energy.

Eur. Phys. J. C (2015) 75:531
DOI 10.1140/epjc/s10052-015-3704-2

Schermature

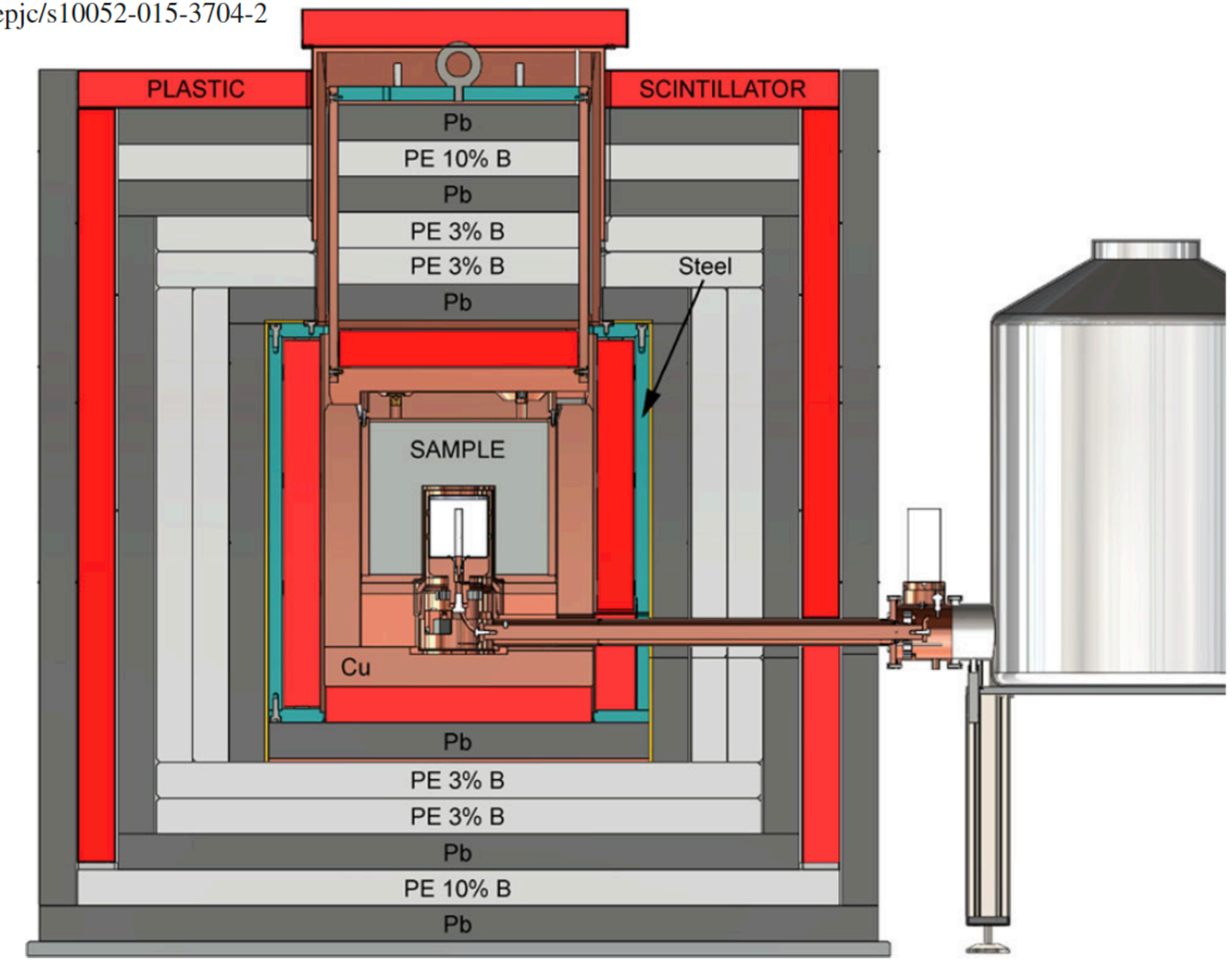

Fig. 1 Cut-away view of the GIOVE detector and shield. Different layers for radiation absorption (Pb, Cu), neutron moderation (PE) and active vetoing (*red colored areas*) form a shell structure to efficiently lower the background count rate in the central Ge crystal. More details provided in the text

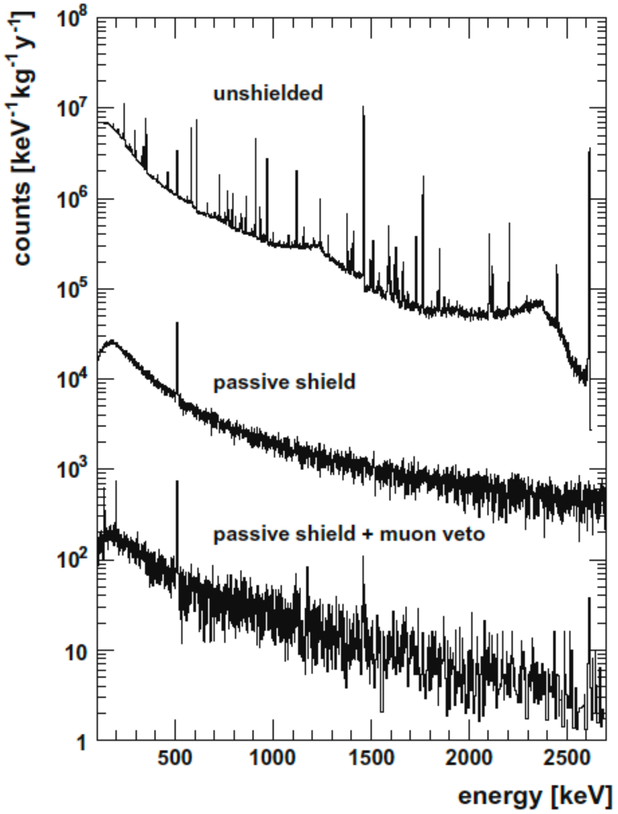

Fig. 9 Spectral background comparison of the GIOVE detector for increasing measures of passive and active shield

Schermature

Table 5 Integral count rates of low-background Ge spectrometers located in different underground sites. The values are normalized by the active mass (m_{act}) of the detectors. Among them, only GIOVE and Corrado are equipped with active muon veto systems. The sample chambers (SC) were empty during the measurement

Detector	m_{act} (kg)	SC_{vol} (liter)	Location, depth (m w.e.)	μ flux reduction (comp. sea level)	Count rate in (40–2700) keV ($d^{-1}kg^{-1}$)
GIOVE	1.81	12.4	MPIK, 15	2−3	348 ± 3
Corrado	0.94	11	MPIK, 15	2−3	3661 ± 11
Ge-3	1.24	0.4	HADES, 500	5×10^3	394 ± 2
GeMPI	2.06	15	LNGS, 3800	10^6	66 ± 1